Journal of Controlled Release 375 (2024) 193–208

Contents lists available at ScienceDirect

Journal of Controlled Release

journal homepage: www.elsevier.com/locate/jconrel

Rational design of a poly-L-glutamic acid-based combination conjugate for hormone-responsive breast cancer treatment

Paz Boix-Montesinos [a], María Medel [a,b], Alessio Malfanti [a,c], Snežana Đorđević [a,b], Esther Masiá [a,b,d], David Charbonnier [a,d,e], Paula Carrascosa-Marco [a], Ana Armiñán [a,b,*], María J. Vicent [a,b,d,*]

[a] Polymer Therapeutics Lab., Príncipe Felipe Research Center, Av. Eduardo Primo Yúfera 3, 46012 Valencia, Spain
[b] Centro de Investigación Biomédica en Red en Cancer, (CIBERONC), Instituto de Salud Carlos III, Spain
[c] Department of Pharmaceutical and Pharmacological Sciences, University of Padova, Via F. Marzolo 5, 35131 Padova, Italy
[d] Screening Platform, Príncipe Felipe Research Center, Av. Eduardo Primo Yúfera 3, 46012 Valencia, Spain
[e] Centro de Investigación Biomédica en Red en Enfermedades Raras (CIBERER), IISCIII and CIEMAT, Madrid, Spain

ARTICLE INFO

Keywords:
Poly-L-glutamic acid
Polypeptide-based combination conjugates
Breast cancer
Cancer spheroids
Patient-derived organoids
Combination therapy

ABSTRACT

Breast cancer represents the most prevalent tumor type worldwide, with hormone-responsive breast cancer the most common subtype. Despite the effectiveness of endocrine therapy, advanced disease forms represent an unmet clinical need. While drug combination therapies remain promising, differences in pharmacokinetic profiles result in suboptimal ratios of free drugs reaching tumors. We identified a synergistic combination of bisdemethoxycurcumin and exemestane through drug screening and rationally designed *star*-shaped poly-L-glutamic acid-based combination conjugates carrying these drugs conjugated through pH-responsive linkers for hormone-responsive breast cancer treatment. We synthesized/characterized single and combination conjugates with synergistic drug ratios/loadings. Physicochemical characterization/drug release kinetics studies suggested that lower drug loading prompted a less compact conjugate conformation that supported optimal release. Screening in monolayer and spheroid breast cancer cell cultures revealed that combination conjugates possessed enhanced cytotoxicity/synergism compared to physical mixtures of single-drug conjugates/free drugs; moreover, a combination conjugate with the lowest drug loading outperformed remaining conjugates. This candidate inhibited proliferation-associated signaling, reduced inflammatory chemokine/exosome levels, and promoted autophagy in spheroids; furthermore, it outperformed a physical mixture of single-drug conjugates/free drugs regarding cytotoxicity in patient-derived breast cancer organoids. Our findings highlight the importance of rational design and advanced in vitro models for the selection of polypeptide-based combination conjugates.

1. Introduction

Hormone-responsive tumors represent the most frequently diagnosed breast cancer subtype [1,2], accounting for ~70 % of all cases. Molecular characterization of these tumors involves evaluating estrogen receptor (ER) expression, which drives hormone-responsive breast cancer cell proliferation [1,3]. The enzyme aromatase catalyzes the synthesis of estrogen [1], which binds to and activates ER to prompt nuclear translocation and gene transcription [4] or interact with cytoplasmic proteins to activate signaling pathways [6]. Overall, ER downstream responses regulate cell cycle progression, cell proliferation, and chemoresistance [1,4].

Therapeutic approaches to hormone-responsive breast cancer include aromatase inhibitors [3] such as exemestane (Exem), an FDA-approved drug widely employed in postmenopausal hormone-responsive breast cancer patients [5]. Despite this success, various cellular mechanisms can prompt therapeutic resistance [1,3]; for instance, ER-independent activation of downstream signaling induces tumor cell growth in the presence of Exem [6]. While resistance processes may arise spontaneously, Exem's off-target side effects contribute to endocrine therapy resistance [7–10]; however, the implementation of an additional drug(s) in combination with Exem may overcome Exem

* Corresponding authors at: Polymer Therapeutics Lab., Príncipe Felipe Research Center, Av. Eduardo Primo Yúfera 3, 46012 Valencia, Spain.
E-mail addresses: aarminan@cipf.es (A. Armiñán), mjvicent@cipf.es (M.J. Vicent).

https://doi.org/10.1016/j.jconrel.2024.09.002
Received 17 June 2024; Received in revised form 20 August 2024; Accepted 1 September 2024
Available online 10 September 2024

resistance [3,11].

Curcuminoids – a family of turmeric-derived compounds – target numerous pathways to affect multiple biological processes and represent candidates for inclusion in hormone-responsive breast cancer therapies [12]. Bisdemethoxycurcumin (BDMC) displays higher stability under physiological conditions than other curcumin/curcuminoid derivatives [13] and represents a candidate for combination therapies with Exem [14]. Unfortunately, both drugs present low water solubility/high degradability (hindering intravenous administration), while differences in pharmacokinetic profiles may result in their arrival at tumor tissues at a suboptimal ratio [13,15].

Conjugating drug combinations to the same nanocarrier can ensure simultaneous delivery to a desired site of action at a controlled ratio [16,17] and improve drug stability/solubility [16,18]; furthermore, conjugation provides advantages such as the bypass of resistance mechanisms due to endocytic internalization [19]. Using stimuli-responsive linkers supports drug stability in circulation *and* site-specific release to avoid off-target effects [20]. Polypeptides represent unique nanocarrier options due to their endogenous-like characteristics and tight synthetic control [20–22], in contrast with synthetic polymeric carriers (e.g., poly(ethylene glycol) or poly(N-(2-hydroxypropyl)methacrylamide) that present limitations regarding their biodegradability and immunogenicity [23,24]. Poly-L-glutamic acid (PGA) offers multivalency (to help fine-tune drug loading and set synergistic drug ratios [20]), biocompatibility, biodegradability, and architectural versatility [21,25]. Branched nanocarriers possess advantages compared to their linear counterparts, such as improved biodistribution and cell trafficking (among notable others) [26]; however, widely employed dendrimers such as poly(amidoamine) and poly(propylene imine) suffer from cytotoxicity [27]. In contrast, star-shaped PGAs (St-PGAs) lack intrinsic cytotoxicity [28] and support increased tumor cell uptake, prolonged blood circulation, and significant tumor accumulation compared to linear PGAs [29].

Rationally selected drugs, loading, ratios, and stimuli-responsive linkers can enhance these polypeptide-based combination conjugates' anti-tumor activity [16]. Previous reports noted that high drug loading prompts a compact conformation, inducing the formation of unimolecular micelles (where drugs locate to the hydrophobic core with the hydrophilic polymer exposed to the aqueous media) that impede linker exposure, hinder drug release, and reduce cytotoxicity [23,30,31]. The drug combination strategy employed also influences therapeutic outcomes [16,21]. A physical mixture of single-drug conjugates provides benefits associated with polypeptide-drug conjugates [16,17] while providing for simpler manufacturing [32,33]; however, conjugate-based combination strategies - conjugating multiple drugs to the same polypeptidic carrier - ensure simultaneous delivery of both drugs to the same cell securing synergism [16,17]. Thus, rational design can help to tailor a conjugate to a disease of interest [21]; additionally, evaluating combination conjugates in faithful preclinical models can accelerate development [34,35].

We synthesized, characterized, and evaluated a St-PGA-based combination therapy for advanced hormone-responsive breast cancer using Exem and BDMC. We maximized therapeutic potential using rational design to select drug loadings/ratios and stimuli-responsive linkers to allow controlled drug(s) release. Physicochemical and drug release characterization revealed that lower drug loading supported optimal drug release in the combination conjugate due to a less compact conjugate solution conformation (as unimolecular micelle). We then used increasingly complex in vitro models to select/characterize candidate combination conjugates, validating efficacy in patient-derived 3D organoids. A low-drug loading combination conjugate demonstrated optimal cytotoxicity synergism in vitro in 3D models compared to combination conjugates with higher loadings or a physical mixture of single-drug conjugates/free drugs; moreover, this candidate modulated mechanisms inhibiting cancer progression and increasing cell death. Overall, the implementation of rational design and complex 3D preclinical models supported the development of a treatment for an unmet clinical need.

2. Materials and methods

Supplementary information (SI) section SI1.1 contains a list of materials used and ethical statements. SI1.2 describes experimental details of physicochemical characterization of poly-L-glutamic acid-based conjugates, cell culture, and treatment evaluation methods.

2.1. Synthesis of poly-L-glutamic acid-based single and combination conjugates

2.1.1. St-PGA-Exemestane synthesis

St-PGA was first derivatized as carbazate (St-PGA-Hz-BOC) to allow Exem conjugation through a hydrazone bond following a previously described approach [30]. Two modification percentages (Exem maximal conjugation of 14 % or 5 % mol) were pursued, and reagent amounts were adjusted accordingly. In brief, St-PGA (150 L-glutamic acid units; molecular weight [Mw] = 129.1 g/mol; 1.0 eq.) was dissolved in 15 ml anhydrous *N*, *N*′-dimethylformamide (DMF) in an inert atmosphere and 4-(4,6-dimethoxy-1,3,5-triazin-2-yl)-4-methyl-morpholinium tetrafluoroborate (DMTMM; 0.20 or 0.07 eq.) was added and the solution stirred for 20 min. Tert-butyl-carbazate (Hz-BOC; 0.15 or 0.05 eq.) was added, and the pH increased to 8 by adding N,N-diisopropylethylamine (DIEA). The resulting solutions were left to react for 24 h at room temperature (RT). Products were precipitated in cold diethyl ether (3 x), and the resultant white powder was dried in a vacuum for 3 h to remove diethyl ether. St-PGA-Hz-BOC was deprotected by dissolving in excess trifluoroacetic acid (TFA) and stirring in a round bottom flask at RT for 30 min. The solution was precipitated in diethyl ether (3 x), washed with water (2 x), and freeze-dried.

The resulting St-PGA-Hz (1.0 eq.) was then dissolved in 10 ml anhydrous DMF under an inert atmosphere, and Exem (0.28 or 0.06 eq.) was added to the solution. 20 μl acetic acid per 100 mg St-PGA-Hz was added, and the reaction was stirred for 48 h at RT. The solution volume was reduced by half, and the crude reaction was purified by an LH-20 Sephadex column (DMF as mobile phase). The first eluting fraction was collected, evaporated up to 1/5 of the initial volume in a vacuum, and precipitated in cold diethyl ether (3 × 100 ml). The resultant yellowish powder was converted into the salt form by adding 5 ml 0.5 M $NaHCO_3$ solution, purified using Vivaspin with cut-off 3 kDa, and lyophilized to yield St-PGA-Exem conjugate as an amorphous white/yellowish solid.

2.1.2. St-PGA-bisdemethoxycurcumin and St-PGA-bisdemethoxycurcumin /Exemestane synthesis

BDMC conjugation was adapted from a previously described approach to yield St-PGA-BDMC and St-PGA-BDMC/Exem conjugates [36]. St-PGA-BDMC synthesis pursued modification at high (6 % mol) or low (1 % mol) BDMC loadings. St-PGA (1.0 eq.) was dissolved in anhydrous DMF in an inert atmosphere, and BDMC (0.08 or 0.03 eq.) was added to the solution, which was cooled in an ice bath for 10 min before adding N-(3-dimethylaminopropyl)-N′-ethylcarbodiimide hydrochloride (EDC; 0.1 or 0.05 eq.) and 4-dimethylaminopyridine (DMAP; 0.05 or 0.01 eq.). St-PGA-BDMC/Exem synthesis pursued maximal BDMC loading at 9 % or 3 % mol for high-loading or 1 % mol for low-loading St-PGA-Exem. St-PGA-Exem (1 eq.) was dissolved in anhydrous DMF in an inert atmosphere for each case. BDMC (0.1, 0.05, or 0.03 eq.) was added to the solution, which was cooled in an ice bath for 10 min before EDC (0.12, 0.07 or 0.05 eq.) and DMAP (0.07, 0.05 or 0.01 eq.) were added. St-PGA-BMDC and St-PGA-BMDC/Exem synthesis followed the same protocol. Reactions were stirred at RT overnight, the volume was reduced by half, and the crude reaction was purified twice by size exclusion chromatography (SEC, Sephadex LH-20 column) with DMF as the mobile phase. The first fraction was evaporated under a

vacuum with 2 ml 0.1 M $NaHCO_3$ solution, redissolved in Milli-Q water, and purified using a Vivaspin 3 kDa cut-off. Final conjugates were collected and freeze-dried as fine yellow/orange powders.

2.2. Physicochemical characterization of poly-L-glutamic acid-based conjugates

2.2.1. Identity confirmation by nuclear magnetic resonance spectroscopy

Proton nuclear magnetic resonance (^{1}H NMR) used salt forms prepared at 1 mg/ml in deuterated water or free drugs at 3 mg/ml in deuterated dimethyl sulfoxide (DMSO).

2.2.2. Determination of total drug loading by ultraviolet-visible spectrometry

Conjugate salt forms were prepared at 1 mg/ml in H_2O. Ultraviolet-visible (UV-VIS) analysis was performed using a JASCO V-630 spectrophotometer 20 at 25 °C with 1.0 cm quartz cells and a spectral bandwidth of 0.5 nm. Spectral analysis was recorded in the 200–600 nm range (3 x). UV-VIS signals for Exem and BDMC were determined at 280 and 405 nm. Drug concentration was derived from a calibration curve obtained using standard solutions of Exem and BDMC in methanol (Fig. S1).

2.2.3. Free drug content analysis by reverse-phase high-performance liquid chromatography

Conjugates were dispersed in acetonitrile and incubated (1 h) before centrifuging the suspension and diluting the supernatant (10 x) with acetonitrile. Free drug (FD) content analysis used reverse-phase high-performance liquid chromatography (RP-HPLC) using the C-18 Lichrospher column.

2.2.4. Determination of size, polydispersity index, and Z-potential by dynamic light scattering

Conjugate solutions (1 mg/ml) were freshly prepared in PBS (10 mM phosphate, 150 mM NaCl) filtered through a 0.45 μm cellulose membrane filter. The polydispersity index (PDI), size distribution (hydrodynamic radius, Rh), and Z-potential were measured for each polymer-drug conjugate using a dynamic light scattering (DLS) ($n \geq 3$, ZetasizerNano ZS (Malvern Panalytical, US).

2.2.5. Drug release kinetics study by liquid chromatography-tandem mass spectrometry

Drug release was assessed at physiological (7.4) and acidic pH (5). Conjugates were dissolved in 20 mM CH_3COONa (pH 5) or Dulbecco's phosphate-buffered saline (DPBS) (pH 7.4) containing 1 μg/ml curcumin as an internal standard. Samples were incubated at 37 °C, and 100 μl aliquots of each conjugate were collected over 72 h. Immediately after collection, samples were frozen in liquid nitrogen and lyophilized overnight. Free drugs were extracted with 100 μl MeOH by mixing and sonicating for 5 min. Samples were centrifuged (11,000 *g*, 10 min) and 90 μl transferred to a liquid chromatography-tandem mass spectrometry (LC-MS/MS) vial with 10 μl 0.1 % formic acid (FA) for analysis (SI).

2.3. Cell culture

2.3.1. 2D monolayer cell culture

MCF7 breast cancer cells - a model for hormone-responsive breast cancer - were cultured in DMEM supplemented with 10 % heat-inactivated fetal bovine serum (FBS) and kept in a humidified incubator (37 °C, 5 % CO_2).

2.3.2. 3D breast cancer cell spheroid culture

Breast cancer cell monolayers were detached using trypsin and resuspended in fresh DMEM. Single-cell suspensions were mixed with 10 mg/ml cold basement membrane extract (BME). Ten 40 μl-droplets of BME containing 10,000 cells/droplet were seeded in six-well suspension plates. Droplets were incubated for 30 min at 37 °C to gel. 3 ml DMEM was added to each well, and spheroids were cultured for eight days.

2.3.3. 3D patient-derived organoid establishment

Breast tumor samples from donors at Fundación Instituto Valenciano de Oncología (FIVO, Valencia, Spain) were used to establish 3D patient-derived organoids adapting a previously published protocol [37] (SI). Briefly, tumor samples were mechanically minced and enzymatically disaggregated before cells were pelleted by centrifugation and erythrocytes were eliminated. $5{\cdot}10^5$ cells were seeded in 40 μl of 10 mg/ml BME in a pre-warmed 24-well plate. After a 30-min incubation at 37 °C, 400 μl of the organoid medium was added, and the medium was changed every 3–4 days. Organoids were used after 14 days when 80 % reached 100 μm in diameter.

2.4. Treatment evaluation in breast cancer monolayer and advanced 3D models

2.4.1. Cell viability

Cells were seeded in 96-well white cell culture plates in 50 μl DMEM at $1.56{\cdot}10^4$ cells/cm^2 for monolayers. For cytotoxicity evaluations in advanced models, spheroids/organoids were generated and harvested as described above. 1000 spheroids/organoids were seeded per well in white, clear bottom 96-well cell culture plates in 40 μl with 10 mg/ml BME. After a 30-min incubation (37 °C, 5 % CO_2) to allow BME to gel, 50 μl DMEM was added to each well. After 24 h for monolayers (to allow cell attachment) and immediately after seeding for spheroids/organoids cultures, 50 μl of DMEM (untreated controls) or DMEM containing serial dilutions of drugs, conjugates, or DMSO (vehicle control) were added. After 72 h, cell viability was measured using MTS (monolayers; during preliminary drug combination ratio selection), CellTiter Glo (monolayers), or CellTiter Glo 3D (organoids/spheroids) following the manufacturer's instructions. Dose-response was presented as cell viability normalized to untreated controls.

2.4.2. Analysis of the mechanism of action of the St-PGA-based conjugates

Ten droplets containing spheroids (per condition) were cultured for eight days. The media was replaced with DMEM (untreated controls) or DMEM-containing drugs, conjugates, or DMSO. After 72 h, spheroids protein extracts were recovered for Western blotting, and the supernatants were snap-frozen and kept for GenieAssay ELISA multiplex assay to detect tumor necrosis factor-alpha (TNF-α), interleukin 6 (IL-6), and interleukin 8 (IL-8) and for AlphaScreen™ exosome (ExoScreen) analysis. Table S1 lists the primary and secondary antibodies used and their optimized dilutions.

2.5. Statistical analysis and data representation

Unless otherwise specified, statistical analysis and data representation were performed in GraphPad Prism 9.0 software (GraphPad, California, USA) with data expressed as mean ± standard error of the mean (SEM). Statistical significance was determined by Student's *t*-test (1-to-1 comparisons) or one-way ANOVA (group comparisons). IC50 values from cytotoxicity treatments were obtained by interpolating dose-response curves fitted to a log(inhibitor) vs. response-variable slope non-linear model. IC50 values for treatments were compared using the extra sum-of-squares F test. When applicable, synergy in combination treatments was studied in CompuSyn (dose-response curves) or SynergyFinder Plus (discrete concentrations).

3. Results and discussion

3.1. Rational selection of St-PGA-based combination conjugate components

We first identified synergistic combinations in MCF7 cells (a model

for hormone-responsive breast cancer). We studied drug combination cytotoxicity and applied the highest single agent (HSA) model, which generates a synergism score (δ score) by comparing drug combination cytotoxicity with the maximum cytotoxicity achieved by the most potent drug within said combination [38] (Fig. S2A). Among the combinations with the highest synergism scores (δ value >20), we selected BDMC and Exem (Fig. 1A), given the ability of BDMC to target pathways associated with Exem resistance.

Effective drug release and maintaining a synergistic drug ratio at a desired site of action relies on drug loading, linking moieties, and the combinatorial strategy employed (as described below) [16,21]. We selected a BDMC:Exem combination ratio that ensured synergism by treating cells with varying concentrations of Exem and BDMC as single agents/in combination, obtaining a dose-response matrix (Fig. S2B). The HSA synergism model again identified synergistic BDMC:Exem ratios (Fig. 1B - a 2D projection of δ values with BDMC:Exem ratio; Fig. S2C - a 3D projection without ratio information). BDMC and Exem synergism/antagonism strongly depended on drug ratio and concentrations (Fig. 1B). Exem induced cell growth at low concentrations (Fig. S2B), perhaps due to induced cytoprotection and signaling pathway activation [7–9]; thus, low Exem concentrations require relatively high counteracting BDMC concentrations to provide synergism (ratios <1:2 for Exem <50 μM) (Fig. 1B). In contrast, Exem reduced cell viability at high concentrations (Fig. S2B); consequently, higher Exem concentrations required low BDMC concentrations for synergism (ratios between 1:2–1:5 for Exem >50 μM) (Fig. 1B).

We aimed to synthesize combination conjugates (St-PGA-BDMC/Exem) containing BDMC and Exem at ratios under 1:2 or between 1:2 and 1:5 to determine effective cytotoxic profiles across multiple drug concentrations in in vitro models. Previous studies highlighted the importance of drug loading in the combination conjugate's final properties [23,30,31]. The synthesis of high-drug loading conjugates (7–14 % mol range) at desired ratios aims to minimize the required dose to achieve cytotoxicity, while a low-drug loading conjugate (2–3 % mol range) at a drug ratio of 1:2–1:5 explores the effect of drug loading. We also aimed to synthesize single-drug conjugates (St-PGA-Exem and St-PGA-BDMC) to explore combination conjugates' therapeutic potential compared to physical mixtures of single-drug conjugates/free drugs (Fig. 1C).

We selected different pH-labile linkers for Exem and BDMC [39] to provide stability at physiological pH and controlled drug release at the acidic pH associated with the tumor microenvironment or the lysosomes [39,40], as St-PGA-based conjugates follow lysosomotropic drug delivery [29]. A previous study reported that hydrazone linkers exhibited the most rapid and highest total release, followed by ester linkers [41]. We hypothesized that a hydrazone linker [Exem] and an ester linker [BDMC] would support more rapid and higher Exem release than BDMC, supporting the maintenance of the selected ratios over release. We previously optimized St-PGA-based BDMC conjugates using pH-labile ester linkers [36,42,43]. Exem contains a carbonyl group (Fig. 1A) enabling conjugation via a hydrazone linker [44], supporting the selection of hydrazone [Exem] and ester [BDMC] linkers as pH-labile linkers that maintain adequate drug ratios upon release.

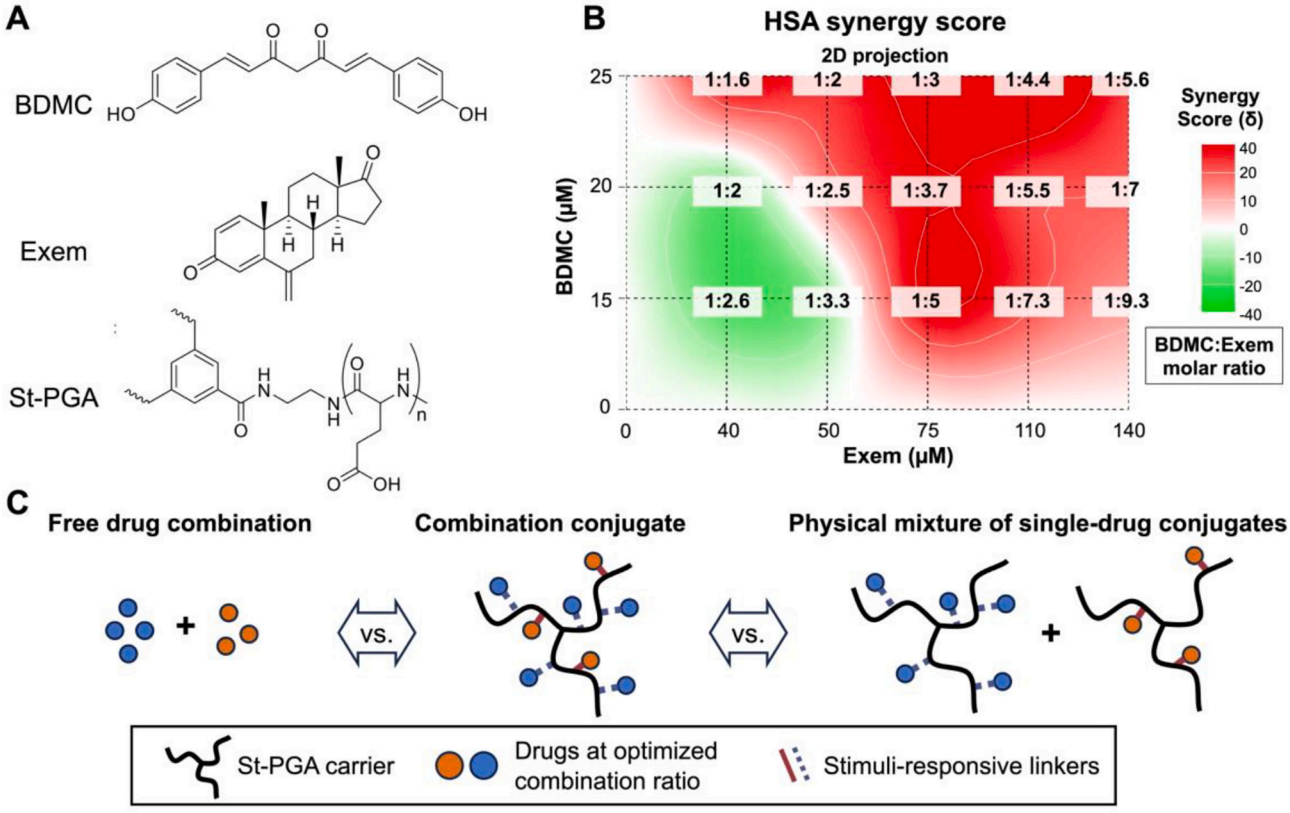

Fig. 1. Rational design of a poly-L-glutamic acid-based combination therapy for hormone-responsive breast cancer treatment. A) Chemical structure of bisdemethoxycurcumin (BDMC), exemestane (Exem), and three-armed *star*-shaped poly L-glutamic acid (St-PGA). B) Synergism scores calculated by the highest single agent (HSA) model obtained from the dose-response matrix by treating MCF7 cell monolayers with BDMC and Exem alone/in combination (dose-response matrix in Fig. S2 where the 3D representation reveals synergy scores (δ) for each combination). δ values of <−10 indicate antagonism, −10-to-10 indicate additivity (lack of synergism/antagonism), and > 10 indicate synergism. The 2D projection contains the same δ information and presents the drug combination ratios for each evaluated concentration (BDMC:Exem molar ratios). White lines connect concentrations presenting equal δ values. C) Schematic representation depicting (middle) a combination St-PGA-based conjugate of Exem and BDMC at an optimized ratio using bioresponsive linkers compared to alternative combination strategies based on a physical mixture of single-drug conjugates (right) or free drugs (left).

3.2. Synthesis and characterization of St-PGA combination and single-drug conjugates

We conjugated BDMC and Exem (alone or in combination) to a three-arm star-shaped carrier, St-PGA (150 glutamic acid units; 50 units per branch). Combination conjugate synthesis began by modifying St-PGA with Hz-BOC (followed by BOC deprotection) for Exem conjugation through a hydrazone linker (Fig. 2A; Fig. S3; representative spectrum shown per synthetic intermediate). We prepared three St-PGA-Exem conjugates at varying drug loadings to serve as single-drug conjugates and combination conjugate precursors (Fig. 2A; Table 1). Combination conjugate synthesis continued by conjugating BDMC through an ester linker, which required carboxylic acid activation using a carbodiimide coupling reagent [36,42,43]. Employing St-PGA-Exem conjugates as starting materials yielded combination conjugates at desired drug loadings/ratios (Fig. 2A; Table 1). For single-drug St-PGA-BDMC conjugates, we conjugated BDMC to St-PGA at high- and low-drug loading (Fig. 2A; Table 1).

We ensured St-PGA-BDMC, St-PGA-Exem, and St-PGA-BDMC/Exem identity using ^{1}H NMR analysis (Fig. 2B; Fig. S4; representative spectrum shown per conjugate). We successfully identified conjugate components in ^{1}H NMR spectra; however, due to NMR's semi-quantitative nature and low signal definition after conjugation, we implemented UV-VIS to determine total drug loading (TDL) [21]. We used calibration curves to quantify Exem and BDMC % mol TDL by determining the maximum absorbance in UV-VIS absorbance peaks (Exem λ_{Max} = 280 nm; BDMC λ_{Max} = 405 nm) (Fig. S1; Table 1). We determined the FD content of conjugates by RP-HPLC to ensure purity, ensuring that drug release studies and biological characterization accurately reflect drug release from conjugates and not impurities. Conjugates presented an FD content <2 % wt TDL, meeting the standard required [45] (Table 1).

We next determined PDI, size distribution, and *Z*-potential values via DLS after dissolving conjugates in PBS (Fig. 2C; Table 1). Conjugates presented narrow molecular distributions (PDI values of 0.2–0.8) and negative Z-potential values (−20 to −30 mV). As expected, drug nature and loading influenced final conjugate size distribution and solution conformation. St-PGA-BDMC$_9$/Exem$_5$, St-PGA-BDMC$_3$/Exem$_7$, and St-PGA-BDMC$_1$/Exem$_3$ displayed Rh values of 5.3, 9.1, and 10.7 nm (Fig. 2C; Table 1; conjugate subindexes = drug loadings). St-PGA-Exem conjugates presented Rh values of 2.4, 2.9, and 3 nm for St-PGA-Exem$_7$, St-PGA-Exem$_5$, and St-PGA-Exem$_3$ (Fig. 2C; Table 1). St-PGA-BDMC$_6$ possessed an Rh value of 5.2 nm (Fig. 2C; Table 1), while St-PGA-BDMC$_1$ reached a significantly higher Rh value of 47.5 nm (Fig. 2C; Table 1).

Overall, conjugates (except for St-PGA-BDMC$_1$) displayed sizes within the 2–14 nm range previously described for unimolecular St-PGA carriers/conjugates [23,29]; however, the larger size of St-PGA-BDMC$_1$ suggests the acquisition of a supramolecular structure after BDMC conjugation (as described below). Exem is a highly hydrophobic and water-insoluble drug that can undergo π-π stacking interactions [13,46]. Exem possesses a more rigid, planar structure than BDMC; therefore, Exem could prompt more significant compaction upon conjugation compared to BDMC, reflected in the smaller size of St-PGA-Exem conjugates (2.4–3 nm range) compared to St-PGA-BDMC/Exem conjugates with the same Exem loading (5.3–10.7 nm range) (Fig. 2D). Moreover, higher drug loading prompted more significant compaction for conjugates of comparable components (Fig. 2D). For St-PGA-BDMC conjugates, the significantly greater size observed with low loading of St-PGA-BDMC$_1$ (47.5 nm) maintains BDMC exposed to the aqueous media and favors the less compact *cis* isomer of BDMC, where phenol-methoxy groups become positioned on the same side of the backbone (Fig. 2E) [47,48]. *Cis* isomers of BDMC could form interactions between other BDMC molecules *between* different conjugates, triggering supramolecular aggregation. In contrast, high BDMC loading (5.2 nm) could induce a compact conformation, favoring the more compact *trans* isomer of BDMC (phenol-methoxy groups become positioned on opposite sides of the backbone [47,48]) (Fig. 2E), maintaining BDMC molecules in the hydrophobic pocket of the conjugate. In St-PGA-BDMC/Exem combination conjugates, BDMC conjugation occurs on St-PGA-Exem (Fig. 2A), resulting in higher BDMC exposure to the aqueous media due to the synthetic sequence and as the Exem loading sterically impedes BDMC from adopting a *cis* isomeric form. Our results agree with previous observations for single- and combination-drug conjugates carrying Dox - a planar molecule with a tendency toward π-π stacking [49]. Polymer-drug conjugates carrying Dox had smaller sizes when compared to an alternative drug with more significant steric effects; moreover, higher Dox loading led to more compact conformations, with Dox "protected" in an intramolecular hydrophobic pocket, hindering exposure to the aqueous media (impeding drug release and limiting cytotoxicity) [17,30].

3.3. Drug(s) release kinetics studies from combination and single-drug conjugates

We studied drug release from combination conjugates and St-PGA-BDMC$_1$ and St-PGA-Exem$_3$ (comparable to St-PGA-BDMC$_1$/Exem$_3$, as detailed below) for comparative purposes at pH 7.4 and 5 [20] (Fig. 3; statistical analyses presented in Fig. S5–7 for purposes of clarity). We first confirmed pH-dependent drug release from combination and single-drug conjugates; overall, conjugates displayed more rapid drug release kinetics at acidic pH (Fig. 3A and B; statistical analysis in Fig. S5). These results confirm linker pH-responsiveness and validate rational design, agreeing with previous observations [41,43,50]; however, drug release kinetics at acidic pH varied considerably *between* conjugates (Fig. 3A and B) potentially due to the conformation-mediated differential exposure of the linkers (discussed below).

We compared drug release from combination conjugates to understand how differences in drug loading and conformation (reflected in size) might affect release; specifically, we focused on drug release profiles at pH 5, representing the tumor microenvironment or the lysosome-associated pH. St-PGA-BDMC$_9$/Exem$_5$ (highest drug loading) presented the lowest drug release at any given time point (30 % total BDMC and 2 % total Exem release after 72 h) (Fig. 3A and B; statistical analysis in Fig. S6). High drug loading in St-PGA-BDMC$_9$/Exem$_5$ could impede linker immolation by protecting Exem within a hydrophobic pocket; conversely, higher BDMC exposure to aqueous media could explain partial BDMC release. In contrast, the lower drug loadings in St-PGA-BDMC$_3$/Exem$_7$ (intermediate drug loading) and St-PGA-BDMC$_1$/Exem$_3$ (lowest drug loading) supported optimal 84 and 71 % total BDMC and 95 and 94 % total Exem release after 72 h (Fig. 3A and B; Fig. S6A and B). Despite reaching comparable total release values, release kinetics from St-PGA-BDMC$_3$/Exem$_7$ and St-PGA-BDMC$_1$/Exem$_3$ differed at early time points (< 24 h) (Fig. 3A and B; Fig. S6A and B). St-PGA-BDMC$_3$/Exem$_7$ released significantly more BDMC than St-PGA-BDMC$_1$/Exem$_3$ from 15 min to 6 h due to a higher exposure of BDMC (Fig. 3A; Fig. S6A), although St-PGA-BDMC$_1$/Exem$_3$ releasing significantly more Exem than St-PGA-BDMC$_3$/Exem$_7$ from 15 min to 6 h, probably due to a less compact core due to the lower Exem loading (Fig. 3B; Fig. S6B). Low drug loadings in St-PGA-BDMC$_1$/Exem$_3$ support accessibility of the drugs/linking moieties to the aqueous medium from early time points; hence, given equal exposure of linkers, the hydrazone linker employed for Exem conjugation could drive rapid Exem release in contrast to slower release facilitated by the ester linker conjugating BDMC for PGA-BDMC$_1$/Exem$_3$, benefiting toward an adequate relative BDMC:Exem release kinetics.

As drug ratio impacts synergism, we explored ratios obtained after drug release from each conjugate at pH 5 over 72 h. St-PGA-BDMC$_9$/Exem$_5$ released BDMC and Exem at a ratio under 1:0.1 at all times (Fig. 3C; obtained from data in Fig. 3A and B). St-PGA-BDMC$_9$/Exem$_5$ possesses drugs at a 1:0.6 ratio (Table 1); therefore, the released ratio represents a five-fold lower value than the conjugated ratio, suggesting minimal cytotoxicity. St-PGA-BDMC$_3$/Exem$_7$ and St-PGA-BDMC$_1$/Exem$_3$ possess drugs at a 1:2.5 ratio (Table 1). Drug release from St-PGA-

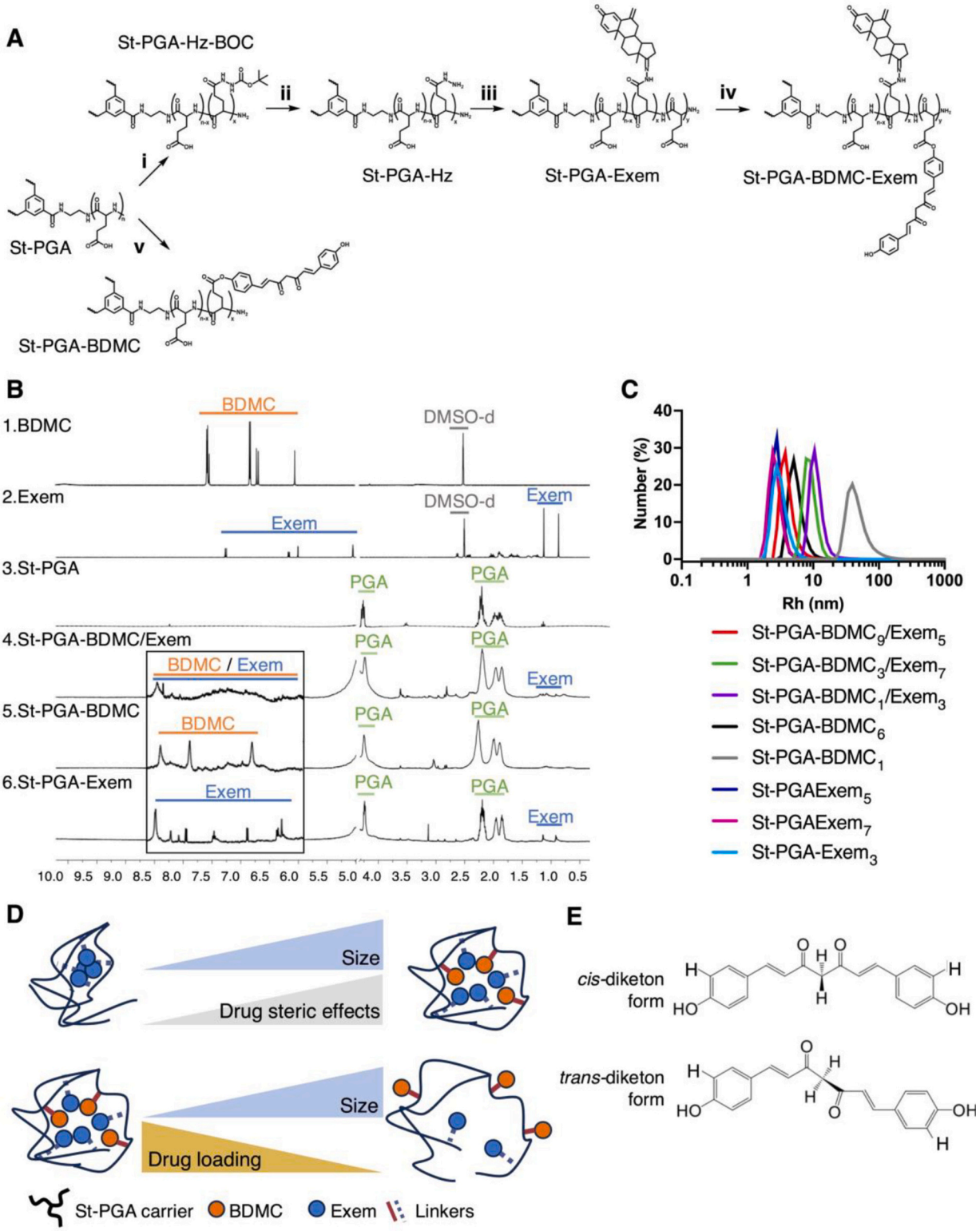

Fig. 2. Synthesis and physicochemical characterization of St-PGA single and combination conjugates. A) Synthetic scheme describing the synthesis of star-shaped poly L-glutamic acid (St-PGA)-based conjugates carrying bisdemethoxycurcumin (BDMC) and exemestane (Exem) alone or in combination. i) DMTMM BF4, N,N-diisopropylethylamine, tert-butyl carbazate, anhydrous DMF, 24 h, RT; ii) trifluoroacetic acid, 30 min, RT; iii) Exem, CH_3COOH, anh-DMF, 48 h, RT; iv and v) BDMC, EDC, DMAP, anhydrous DMF, 16 h, ice bath. B) Representative ^1H NMR spectra of BDMC, Exem, St-PGA, and single-drug and combination conjugates (Fig. S4 identifies the specific protons in the chemical structure of molecules generating each signal). The black square delimits a magnified area, allowing more precise visualization of peaks at the 6.0 to 8.6 ppm region. The 5.0 to 4.6 ppm region was removed to eliminate the deuterated water signal and improve spectra resolution. DMSO-*d* = deuterated DMSO. C) St-PGA-based conjugate sizes measured by dynamic light scattering. Size distribution graphs expressed as the number of molecules (%) per hydrodynamic radius (Rh) obtained by dynamic light scattering in phosphate-buffered saline at 2.0 mg/ml. D) Proposed model for conjugates with size directly correlating drug steric hindrance (top) and inversely correlating drug loading (bottom) in an aqueous solution. E) Chemical structure of bisdemethoxycurcumin conformational isomers.

Table 1
Summary of the physicochemical descriptors of St-PGA-based combination and single-drug conjugates.

Compound name	BDMC loading (% mol)*	Exem loading (% mol)*	Molar ratio (BDMC: Exem)	Size** (Rh, nm ± SEM)	PDI** (± SEM)	*Z*-pot** (mV, ± SEM)	FD (% wt to TDL)	
							BDMC	Exem
Combination conjugates								
St-PGA-$BDMC_9$/ $Exem_5$	9.1	5.0	1:0.6	5.3 ± 1.4	0.47 ± 0.01	−17.4 ± 0.7	0.98	1.02
St-PGA-$BDMC_3$/ $Exem_7$	2.8	7.0	1:2.5	9.1 ± 2.2	0.29 ± 0.01	−31.1 ± 0.4	1.05	0.90
St-PGA-$BDMC_1$/ $Exem_3$	1.2	2.9	1:2.5	10.8 ± 1.2	0.29 ± 0.02	−28.0 ± 1.0	0.35	0.152
Single-drug conjugates								
St-PGA-$BDMC_6$	6.8	n/a	n/a	5.2 ± 0.7	0.66 ± 0.03	−19.4 ± 1.0	1.40	n/a
St-PGA-$BDMC_1$	1.2	n/a	n/a	47.5 ± 0.9	0.22 ± 0.01	−34.4 ± 0.8	0.46	n/a
St-PGA-$Exem_7$	n/a	7	n/a	2.4 ± 0.2	0.78 ± 0.01	−28.3 ± 1.0	n/a	1.01
St-PGA-$Exem_5$	n/a	5	n/a	2.9 ± 0.3	0.37 ± 0.04	−17.4 ± 0.7	n/a	<0.2***
St-PGA-$Exem_3$	n/a	2.9	n/a	3.0 ± 0.2	0.73 ± 0.07	−17.9 ± 1.2	n/a	0.23

BDMC = Bisdemethoxycurcumin; Exem = Exemestane; FD = free drug; n/a = not applicable; PDI = polydispersity index; Rh = hydrodynamic radius; St-PGA = *star*-shaped poly-L-glutamic acid; TDL = total drug loading; wt = weight; Z-pot = Z-potential.
* Obtained by UV-VIS.
** Obtained by DLS.
*** Below limit of quantification.

$BDMC_3$/$Exem_7$ increased slowly, maintaining a ratio below 1:2 until 24 h and reaching a plateau of 1:2.5 after 24 h (Fig. 3C). Drug release from St-PGA-$BDMC_1$/$Exem_3$ supported a rapidly increasing ratio, reaching 1:2–1:5 (within the target range) from 1 h and increasing to 1:5.3 at 6 h before decreasing to a plateau of 1:3 maintained until 72 h (Fig. 3C). Maintaining an optimal drug ratio from early time points may represent an advantage for St-PGA-$BDMC_1$/$Exem_3$.

We next evaluated potential differences in the release of multiple drugs conjugated to the same carrier compared to those conjugated to independent carriers [13,46]. Combination conjugates and St-PGA-Exem conjugates presented similar drug loading due to their common synthetic origin (Fig. 2A); however, we synthesized St-PGA-BDMC conjugates independently, and they acquired similar, but not necessarily equal, drug loading. St-PGA-$BDMC_1$ and St-PGA-$Exem_3$ present the same individual drug loadings as St-PGA-$BDMC_1$/$Exem_3$; thus, we expect that any differences could inform how one drug's release may impact the other. We observed comparable BDMC release from St-PGA-$BDMC_1$/$Exem_3$ and St-PGA-$BDMC_1$ at all time points (Fig. 3A and B; statistical analysis in Fig. S7A); in contrast, Exem release differed significantly, with significantly higher release observed from St-PGA-$BDMC_1$/$Exem_3$ at all time points (Fig. 3B; Fig. S7B). While St-PGA-$BDMC_1$/$Exem_3$ supported 96 % Exem release at 72 h, St-PGA-$Exem_3$ released a significantly lower level of release (55 %) (Fig. 3B; Fig. S7B).

Our drug release kinetics study from combination conjugates demonstrated a correlation between lower loading and optimal release. The combination conjugate with the highest drug loading (St-PGA-$BDMC_9$/$Exem_5$) showed low total drug release and low drug combination ratio; in contrast, combination conjugates at lower drug loadings (St-PGA-$BDMC_3$/$Exem_7$ and St-PGA-$BDMC_1$/$Exem_3$) presented optimal total drug release, with the combination conjugate at the lowest drug loading (St-PGA-$BDMC_1$/$Exem_3$) demonstrating optimal drug ratio from early time points. Importantly, our results also suggest that BDMC conjugation reduces the compactness of the conformation acquired by St-PGA-Exem, highlighting the advantage of combination conjugates compared to single-drug counterparts and providing evidence that BDMC conjugation supports drug exposure to the aqueous media (in single-drug and combination conjugates).

3.4. Evaluation of St-PGA-based conjugate therapeutic potential in breast cancer cell monolayer culture

We next evaluated the synergism of rationally designed combination conjugates by exposing MCF7 cell monolayer (simplistic and cost-effective) to combination and single-drug conjugates, with the free drugs (individually or combined) as control. St-PGA-based conjugates internalize following the endocytic pathway [29], where they encounter the low pH conditions of lysosomes (pH ≈ 5) that trigger drug release. We calculated IC50 (Table 2) and combination index (CI) values to characterize synergism (CI < 1), additivity (CI ≈ 1), or antagonism (CI > 1).

We compared the cytotoxicity/synergism of combination conjugates with corresponding physical mixtures of single-drug conjugates/free drugs (Fig. 4A-F; Fig. S8A-C - cytotoxicity expressed in Exem equivalents). We compared combination conjugates with higher drug loadings (PGA-$BDMC_9$/$Exem_5$ and PGA-$BDMC_3$/$Exem_7$) to St-PGA-$BDMC_6$ and the lowest drug loading (St-PGA-$BDMC_1$/$Exem_3$) to St-PGA-$BDMC_1$ for the corresponding physical mixtures of single-drug conjugates. All combination conjugates resulted in higher cytotoxicity and synergism than the corresponding physical mixtures of single-drug conjugates (Fig. 4A-F). The high-drug loading combination conjugate (St-PGA-$BDMC_9$/$Exem_5$) provided decreased cytotoxicity/synergism compared to the physical mixture of free drugs (Fig. 4B); in contrast, intermediate- (St-PGA-$BDMC_3$/$Exem_7$) and low-drug loading (St-PGA-$BDMC_1$/$Exem_3$) combination conjugates outperformed the cytotoxicity/synergism of free drug physical mixture (Fig. 4D and F). St-PGA-mediated drug delivery to cells could explain the benefit of combination conjugates through, for example, the bypass of resistance mechanisms involving multidrug-resistance (MDR) pump activity [51] or co-delivery of drugs at optimized drug ratios [16,52]. Studies have reported the superiority of conjugating drugs to the same polymeric carrier over a mixture of corresponding single-drug conjugates [31,53] when the drugs benefit from simultaneous delivery and share the target cell.

A direct comparison of cytotoxicity/synergism between combination conjugates (Fig. 4G and H; cytotoxicity expressed in Exem equivalents in Fig. S8D) confirmed the significantly lower cytotoxicity of St-PGA-$BDMC_9$/$Exem_5$ compared to St-PGA-$BDMC_3$/$Exem_7$ and St-PGA-$BDMC_1$/$Exem_3$ (which displayed comparable cytotoxicity) (Fig. 4G); moreover, we confirmed distinct synergism profiles, with St-PGA-$BDMC_9$/$Exem_5$ displaying increased antagonism with concentration, St-PGA-$BDMC_3$/$Exem_7$ ranging from additivity to synergism, and St-PGA-$BDMC_1$/$Exem_3$ displaying synergism at all concentrations (Fig. 4H). These results agree with the combination conjugate drug release data (Fig. 3A and B; Fig. S6), where St-PGA-$BDMC_1$/$Exem_3$ released drugs at an optimal drug ratio at earlier time points than St-PGA-$BDMC_3$/$Exem_7$ (Fig. 3C), which may explain the increased synergism of St-PGA-$BDMC_1$/$Exem_3$ at all concentrations.

The cytotoxicity of single-drug conjugates as independent treatments supported the observed correlation between conjugate loading/

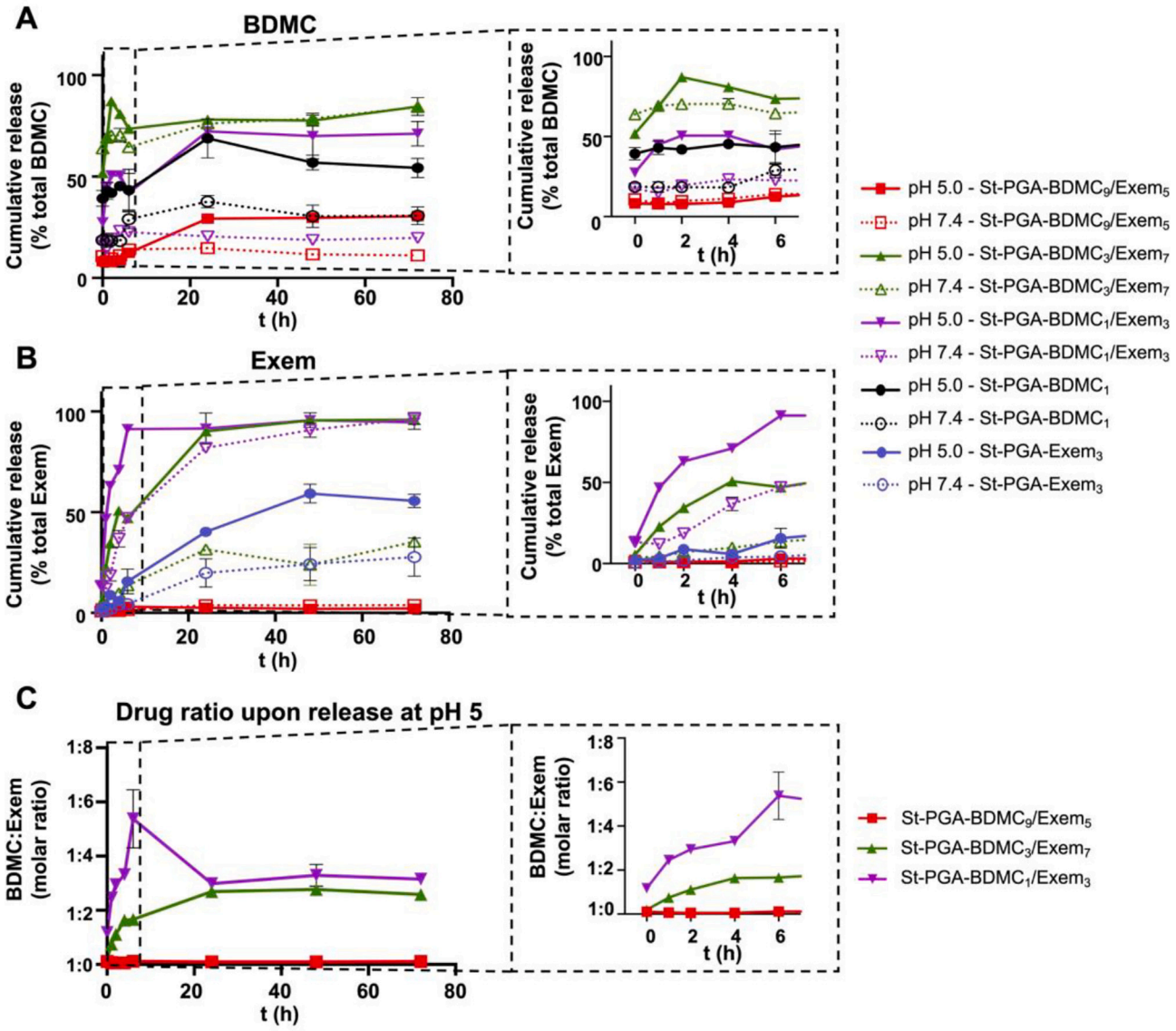

Fig. 3. Drug release kinetic profiles of St-PGA single and combination conjugates. (A) BDMC or (B) Exem release at pH 5 and 7.4 from the St-PGA-$BDMC_9$/$Exem_5$, St-PGA-$BDMC_3$/$Exem_7$, and St-PGA-$BDMC_1$/$Exem_3$ combination conjugates and the St-PGA-$BDMC_1$ and St-PGA-$Exem_3$ single-drug conjugates. Data represented as the percentage of free drugs normalized to total drug loading. Data shown as mean ± SEM of two independent experiments comprising two independent quantifications each ($n = 2$) for combination conjugates or three independent experiments for single-drug conjugates ($n = 3$). The magnified area provides a more precise visualization of the 0–6 h time points. Fig. S5-S7 report statistical analyses of the data in individual figures for more precise visualization. C) Ratio of released drugs from combination conjugates over 72 h at pH 5. Data calculated as molar drug combination ratio (Exem:BDMC mol:mol) from the drug release profile at each time point represented in A and B.

composition and conformation (Fig. 2C). St-PGA-$BDMC_6$ presented lower cytotoxicity than BDMC (Fig. 4A and C), with St-PGA-$BDMC_1$ presenting higher cytotoxicity than BDMC (Fig. 4E). The improved cytotoxicity of St-PGA-$BDMC_1$ could derive from higher BDMC stability afforded by conjugation [54], while the reduced cytotoxicity of St-PGA-$BDMC_6$ could derive from the compact conformation that protects BDMC (Fig. 2C). St-PGA-$Exem_5$ (Fig. S8A), St-PGA-$Exem_7$ (Fig. S8B), and St-PGA-$Exem_3$ (Fig. S8C) failed to reduce cell viability under 50 %, presenting lower cytotoxicity than Exem. These results provide evidence for a tendency for conformation compaction in St-PGA-Exem conjugates, which protects Exem and hinders release.

Our evaluations of cytotoxicity/synergism in cell monolayers confirmed combination conjugates as a more promising strategy than physical mixtures of single-drug conjugates/free drugs; moreover, combination conjugates at lower drug loading induced higher cytotoxicity/synergism due to the adopted conjugate solution conformation yielding to adequate drug(s) release kinetics, providing the desired drug bioavailability and an adequate ratio that secures synergism.

3.5. *Evaluation of St-PGA-based conjugate therapeutic potential in breast cancer 3D cell spheroids*

Monolayer cell cultures do not fully recapitulate the characteristics of in vivo tumors and lack an extracellular matrix (ECM) [35]. In this sense, cell line-based spheroids cultured in ECM-like matrices (such as BME) represent more faithful tumor models, recapitulate relevant cell-cell/cell-matrix interactions [35,55], demonstrate higher chemoresistance, and hence may serve as an improved screen for therapeutics [35,56]. MCF7 cells repeatably formed compact, round spheroids with similar growth rates between independent experiments and mean diameters of 77.20 ± 1.08 μm (Fig. S9). Following an equivalent strategy as for monolayers, we treated spheroids with combination conjugates

Table 2
IC50 values of St-PGA-based conjugates and free drugs in monolayer cultures.

Compound name	IC50 (μM BDMC eq.)	IC50 (μM Exem eq.)	Molar ratio (BDMC:Exem)
BDMC	29.2 ± 1.4	n/a	n/a
Exem	n/a	156.0 ± 1.2	n/a
BDMC + Exem (1:0.6)	28.3 ± 1.4	19.7 ± 1.2	1:0.6
BDMC + Exem (1:2.5)	20.1 ± 1.3	50.2 ± 1.1	1:2.5
St-PGA-$BDMC_9$/$Exem_5$	48.5 ± 1.6	29.1 ± 1.20	1:0.6
St-PGA-$BDMC_3$/$Exem_7$	14.7 ± 1.2	35.9 ± 1.21	1:2.5
St-PGA-$BDMC_1$/$Exem_3$	13.4 ± 1.3	33 ± 1.3	1:2.5
St-PGA-$BDMC_6$ + St-PGA-$Exem_5$	78.0 ± 2.1	46.8 ± 1.2	1:0.6
St-PGA-$BDMC_6$ + St-PGA-$Exem_7$	59.0 ± 1.8	147.0 ± 1.2	1:2.5
St-PGA-$BDMC_1$ + St-PGA-$Exem_3$	31.0 ± 1.6	77.5 ± 1.21	1:2.5
St-PGA-$BDMC_6$	83 ± 1.4	n/a	n/a
St-PGA-$BDMC_1$	18 ± 1.4	n/a	n/a
St-PGA-$Exem_7$	n/a	n/d	n/a
St-PGA-$Exem_5$	n/a	n/d	n/a
St-PGA-$Exem_3$	n/a	n/d	n/a

BDMC = Bisdemethoxycurcumin; Exem = Exemestane; n/a = not applicable; n/d = not detected.

and single-drug conjugates/free drugs (individual/combined). Of note, the low cytotoxicity of various treatments hindered IC50 value calculation, statistical comparisons, and CI curve characterization.

We first compared cytotoxicity/synergism in cell spheroids for combination conjugates with corresponding physical mixtures of single-drug conjugates/free drugs (Fig. 5A-C; cytotoxicity expressed in Exem equivalent concentration in Fig. S10A-C). St-PGA-$BDMC_9$/$Exem_5$ (high drug loading) displayed comparably lower cytotoxicity than a physical mixture of St-PGA-$BDMC_6$ and St-PGA-$Exem_5$ or free drugs (1:0.6 ratio) (Fig. 5A; Fig. S10A). St-PGA-$BDMC_3$/$Exem_7$ (intermediate loading) displayed higher cytotoxicity than a physical mixture of St-PGA-$BDMC_6$ and St-PGA-$Exem_7$ – which induced cell growth, resulting in antagonism (Fig. 5B; Fig. S10B), potentially due to cytoprotective effects exerted by Exem at low concentrations, enhanced due to the higher chemoresistance of spheroids. St-PGA-$BDMC_3$/$Exem_7$ displayed lower cytotoxicity than a physical mixture of free drugs (1:2.5 ratio) (Fig. 5B; Fig. S10B). St-PGA-$BDMC_1$/$Exem_3$ (low drug loading) displayed higher cytotoxicity than a physical mixture of St-PGA-$BDMC_1$ and St-PGA-$Exem_3$, and comparable cytotoxicity to a physical mixture of free BDMC and Exem (1:2.5 ratio) (Fig. 5C; Fig. S10C).

While St-PGA-$BDMC_9$/$Exem_5$ constituted an exception due to low cytotoxicity, St-PGA-$BDMC_3$/$Exem_7$ and St-PGA-$BDMC_1$/$Exem_3$ demonstrated improved cytotoxicity in spheroids compared to corresponding physical mixtures of single-drug conjugates. Combination conjugates carry both drugs together while crossing complex barriers (e.g., the ECM, cell mass, and cell membranes [35]), while single-drug conjugates must overcome each barrier independently; thus, spheroids may provide a more faithful representation of the in vivo setting. In spheroids, combination conjugates presented lower (St-PGA-$BDMC_3$/$Exem_7$) or comparable (St-PGA-$BDMC_1$/$Exem_3$) cytotoxicity than a physical mixture of free drugs. In contrast, these combination conjugates demonstrated higher cytotoxicity than a physical mixture of free drugs in monolayers (Fig. 4B and C). The differential result between cell models could derive from the recapitulation of ECM composition/structure in spheroids, representing a barrier that hinders nanomedicine diffusion to a greater extent than free drugs [57]. To envision how these results could translate to the in vivo setting, we must consider that in vitro models represent a static scenario that does not represent nanomedicine clearance. Slow penetration through the in vitro ECM may delay drug arrival at tumor cells (hindering in vitro cytotoxicity); however, slower penetration through the in vivo ECM could prevent rapid tumor clearance [58], thereby enhancing treatment efficacy. Thus, in vitro models cannot fully reproduce the complexity of the tumor response, and these limitations should be considered. Finally, the direct comparison of cytotoxicity/synergism between combination conjugates in spheroids (Fig. 5D; cytotoxicity expressed in Exem equivalent concentration in Fig. S10D) confirmed the higher cytotoxicity of St-PGA-$BDMC_1$/$Exem_3$ compared to both St-PGA-$BDMC_9$/$Exem_5$ and St-PGA-$BDMC_3$/$Exem_7$.

Overall, these data suggested that St-PGA-$BDMC_1$/$Exem_3$ outperforms St-PGA-$BDMC_9$/$Exem_5$ and St-PGA-$BDMC_3$/$Exem_7$ in 3D spheroid cultures of breast cancer cells. In contrast, St-PGA-$BDMC_1$/$Exem_3$ presented comparable cytotoxicity to St-PGA-$BDMC_3$/$Exem_7$ in cell monolayers (Fig. 4D); thus, the novel differences encountered in the 3D model highlight that more complex models can amplify differences between nanomedicines, aiding the selection of the most promising candidate to undergo further characterization. We conclude that St-PGA-$BDMC_1$/$Exem_3$ represents the most promising candidate for hormone-responsive breast cancer treatment and hence selected this combination conjugate for subsequent investigations.

3.6. *Understanding combination conjugate synergism in breast cancer 3D cell spheroids*

We aimed to study intersecting pathways and biological processes regarding the mechanisms of action of BDMC and Exem in cell spheroids, which may help describe their synergistic activity.

3.6.1. *St-PGA-$BDMC_1$/$Exem_3$ modulates key signaling pathways toward an efficient anticancer effect*

Few studies explore the mechanism of action of Exem or BDMC in hormone-responsive cancer cells; however, previous reports demonstrated that Exem activates ERK independently of ER signaling, which can prompt endocrine resistance [9,65], and highlighted Exem-induced autophagy as a cytoprotective mechanism [8,10]. The demonstrated anti-tumorigenic potential of a combination of Exem with an androgen receptor agonist relied on the blockade of Ras/MEK/ERK and PI3K/Akt/mTOR signaling [7]. Various reports suggest the potential of curcuminoids to downregulate Ras/MEK/ERK and PI3K/Akt/mTOR proliferation-associated signaling pathways [12,59]; moreover, BDMC and other curcuminoids represent known autophagy inducers [59,60]. Low levels of autophagic activity represent a compensatory mechanism that aids breast cancer cell survival [8], while elevated levels promote active cancer cell death [60,61]. Thus, these proliferation-associated signaling pathways and the activation of autophagy are affected by Exem and BDMC and could constitute different axes driving synergism.

We treated spheroids with St-PGA-$BDMC_1$/$Exem_3$ and single-drug conjugates/free drugs (individual/combined) and included an untreated control (for St-PGA-based treatments; media) and a DMSO-treated control (for free drugs; DMSO-containing media). We examined the phosphorylation (indicative of activation) of ERK and mTOR signaling pathway proteins to explore pathway activation [4,62]. We studied the ratio of the microtubule-associated protein light chain 3 (LC3)-II to total LC3 levels (which reflect autophagosome formation [61,63]), indicating autophagy modulation. We confirmed that DMSO and untreated controls yielded comparable results (discounting solvent-derived effects on conclusions) and compared treatments with corresponding controls. We compared treatments with St-PGA-$BDMC_1$/$Exem_3$ to explore potentially improved combination conjugate candidate cytotoxicity in spheroids via the modulation of relevant pathways/biological processes.

Previous reports reported that Exem activates ERK independently of ER signaling, which can prompt endocrine resistance [9,64]. Increased p-ERK levels upon Exem treatment failed to reach statistical significance, while St-PGA-$Exem_3$ prompted a significant increase in p-ERK levels (Fig. 5E - representative Western Blot; Fig. S11 - uncropped Western blot membranes; Fig. 5F - densitometry quantitation). Treatment with non-Exem-containing treatments (BDMC and St-PGA-$BDMC_1$) failed to increase p-ERK levels (Fig. 5F). St-PGA-$BDMC_1$/$Exem_3$

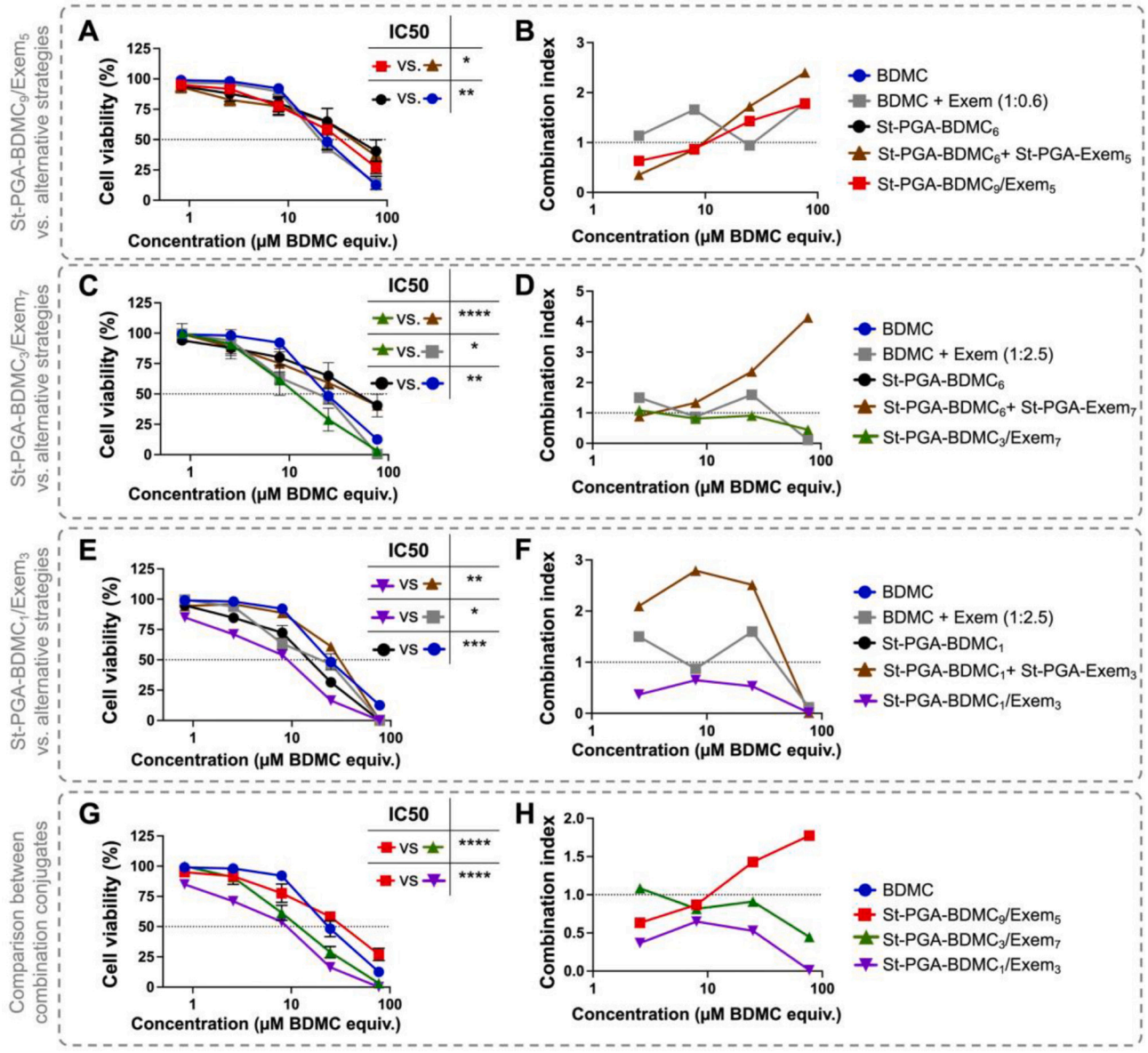

Fig. 4. Evaluation of the cytotoxicity and synergism of poly-L-glutamic acid-based combination/single-drug conjugates in breast cancer cell monolayers. A, C, E, and G describe dose-response curves of MCF7 cell monolayers incubated for 72 h with combination conjugates, single-drug conjugates, and free drugs (individually or combined). Data represented as mean ± SEM of three independent biological replicates ($n = 3$). Concentrations represented in BDMC-equivalents according to drug loading (Exem-equivalents in Fig. S8). Statistical analysis performed using an extra sum-of-squared F test fit comparison for IC50 values. B, D, F, and H describe combination index (CI) curves for combination conjugates and single-drug-conjugate and free-drug combinations. CI calculated from dose-response curve data using CompuSyn. A-F compares combination conjugates to corresponding single-drug conjugates/free drugs combined at a ratio. G and H report a comparison of combination conjugates. Statistical significance of relevant comparisons represented as p-value <0.05 (*), p-value <0.01 (**), p-value <0.001 (***), and p-value <0.0001 (****) following the colour code presented in the legend.

maintained low p-ERK levels, with levels not significantly differing compared to St-PGA-BDMC$_1$, BDMC, or Exem (Fig. 5F). In contrast, a physical mixture of single-drug conjugates/free drugs prompted a significant increase in p-ERK levels (Fig. 5F). Maintaining a synergistic combination via simultaneous drug delivery may, therefore, represent the primary mechanism inhibiting ERK signaling. A physical mixture of St-PGA-BDMC$_1$ and St-PGA-Exem$_3$ induced significantly higher p-ERK levels than St-PGA-BDMC$_1$/Exem$_3$ (Fig. 5F). Although not statistically significant, St-PGA-BDMC$_1$/Exem$_3$ maintained reduced p-ERK levels compared to a physical mixture of BDMC and Exem or St-PGA-Exem$_3$ (Fig. 5F). Thus, St-PGA-BDMC$_1$/Exem$_3$ prevented ERK activation, thereby impeding the potential induction of endocrine-based therapy resistance.

The p70S6 kinase (p70) acts as an effector after phosphorylation (p-p70) and represents the most well-characterized mTORC1 target [65]. As this proliferation-associated pathway is often active in breast cancer cells, downregulation represents a therapeutic strategy [66]. Compared to respective controls, Exem, St-PGA-Exem$_3$, St-PGA-BDMC$_1$/Exem$_3$, and a physical mixture of St-PGA-BDMC$_1$ and St-PGA-Exem$_3$ significantly reduced p-p70 levels, while BDMC, St-PGA-BDMC$_1$, or a physical mixture of BDMC and Exem maintained p-p70 levels comparable to respective controls (Fig. 5E - representative Western Blot; Fig. S11 - uncropped Western blot membranes; Fig. 5G - densitometry quantitation). St-PGA-BDMC$_1$/Exem$_3$ treatment significantly reduced p-p70 levels compared to all treatments except Exem or a physical mixture of St-PGA-BDMC$_1$ and St-PGA-Exem$_3$ (Fig. 5G). These data indicate that St-PGA-BDMC$_1$/Exem$_3$ and a physical mixture of St-PGA-BDMC$_1$ and St-PGA-Exem$_3$ effectively reduced p-p70 levels, suggesting proliferation-

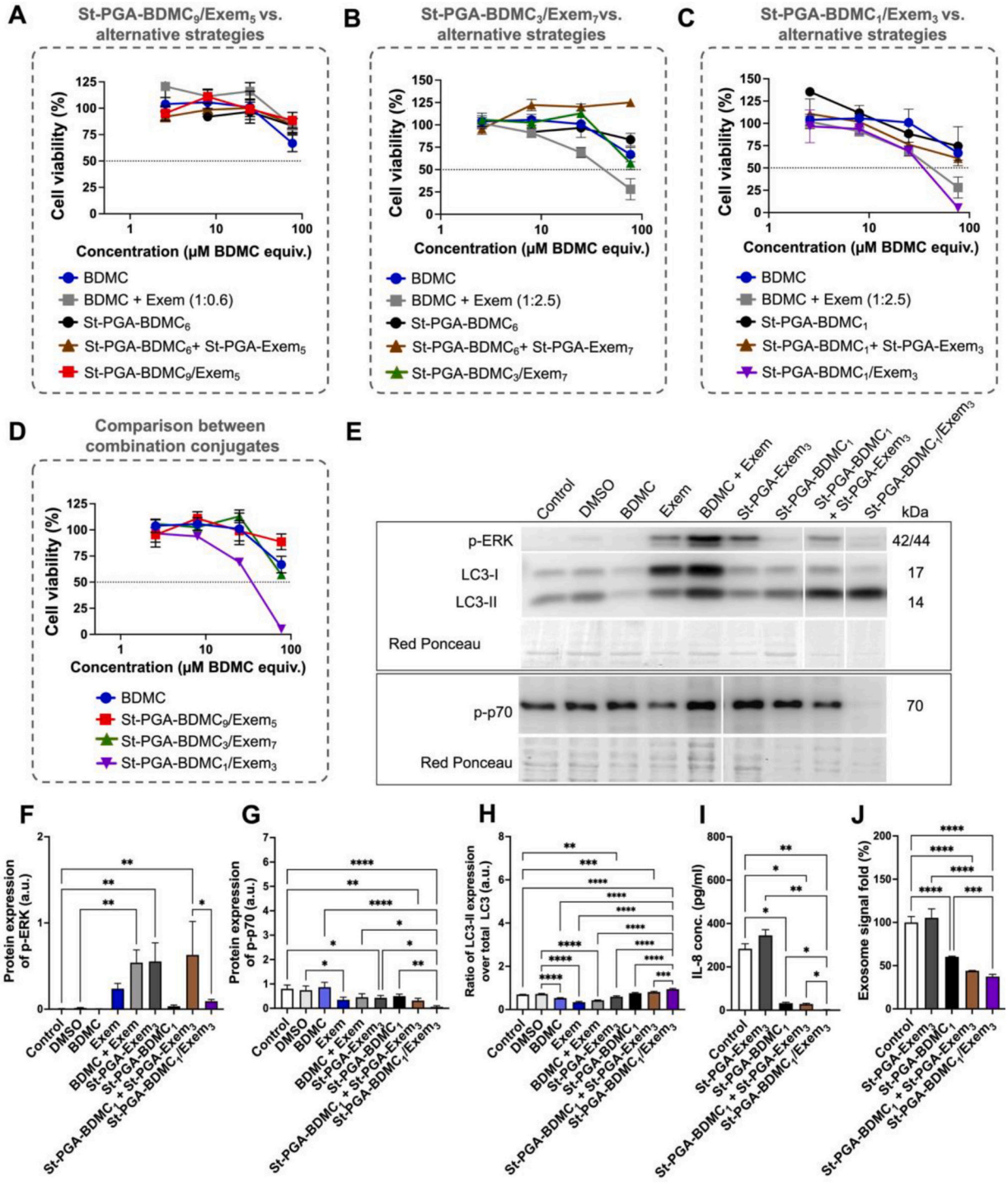

Fig. 5. Evaluation of the cytotoxicity, synergism, and mechanism of action of poly-L-glutamic acid-based combination/single-drug conjugates in breast cancer cell spheroids. A-D) Dose-response curves of MCF7 cell spheroids incubated for 72 h with combination conjugates and single-drug conjugates/free drugs (individually or combined). Concentrations represented at BDMC-equivalent according to drug loading. A-C present individual dose-response curves of each combination conjugate and corresponding single-drug conjugates/free drugs combined at corresponding ratios for (A) St-PGA-BDMC$_9$/Exem$_5$, (B) St-PGA-BDMC$_3$/Exem$_7$, and (C) St-PGA-BDMC$_1$/Exem$_3$. D presents a comparison between combination conjugates. Data represented as mean ± SEM of three independent biological replicates ($n = 3$). Low cytotoxicity hindered IC50 visualization of treatments and, consequently, statistical analysis by extra sum-of-squared F test fit comparison for IC50 values in A, B, and D. Statistical analysis performed using an extra sum-of-squared F test fit comparison for IC50 values in C. E) Representative Western blot images for LC3BI (14 kDa), LC3BII (18 kDa), phosphorylated ERK (p-ERK) (42–44 kDa), and phosphorylated p70 (p-p70) (70 kDa); total protein stained by Red Ponceau staining used as the loading control. Lane order has been altered (see gaps between moved lanes; Fig. S11 contains the original uncropped membranes). DMSO serves as a control for BDMC and Exem, as single drugs and combined. Untreated controls ("control") serve as controls for St-PGA-based conjugates. F—H) Densitometry quantification normalized by Red Ponceau total protein in Western blotting. I and J) Measurement of (I) interleukin-8 (IL-8) levels (GeniePlex Multiplex Assay) or (J) exosomes (ExoScreen™) into the supernatant of MCF7 cell spheroids incubated for 72 h with St-PGA-BDMC$_1$/Exem$_3$ or corresponding single-drug conjugates. Free drug treatments from I and J not shown due to a DMSO-induced solvent effect are presented in Fig. S12 and 13. For graph F-J, statistically significant differences between each treatment and corresponding controls or St-PGA-BDMC$_1$/Exem$_3$ identified by one-way ANOVA represented as p-value<0.05 (*), <0.01 (**), p-value <0.001 (***), and p-value <0.0001 (****). (For interpretation of the references to colour in this figure legend, the reader is referred to the web version of this article.)

associated PI3K/Akt/mTOR pathway downregulation. While Exem significantly reduced p-p70 levels, conjugate-based treatments would provide additional advantages [19,21].

We also explored autophagy by quantifying the LC3-II ratio relative to total LC3 (I + II). Comparing treatments to respective controls revealed that free drugs (individual/combined) and St-PGA-$Exem_3$ reduced, St-PGA-$BDMC_1$ maintained, and St-PGA-$BDMC_1$/$Exem_3$ and a physical mixture of St-PGA-$BDMC_1$ and St-PGA-$Exem_3$ increased the LC3-II ratio (Fig. 5E - representative Western Blot; Fig. S11 - uncropped Western blot membranes; Fig. 5H – LC3-II ratio derived from LC3-II and LC3-III densitometry). St-PGA-$BDMC_1$/$Exem_3$ resulted in the highest LC3-II ratio, suggesting significantly increased autophagosome formation (Fig. 5H). The blockade of autophagy - a complex cyclic process - prompts the accumulation of autophagosomes; therefore, LC3-II accumulation could result from autophagy inhibition [63]; nevertheless, the activation of autophagy by BDMC and Exem treatment has been widely reported [8] which supports that our observation derived from autophagy upregulation. Our data suggest that free drugs (individual/combined) and single-drug conjugates (individually) reduce/maintain autophagic activity. The contrasting results may derive from a drug dose under a trigger threshold. In contrast, a physical mixture of single-drug conjugates and the combination conjugate increases autophagic activity, which can contribute to active cell death. We observed increased LC3-II and decreased p-ERK levels upon St-PGA-$BDMC_1$/$Exem_3$ treatment. LC3-II and p-ERK levels correlate in the absence of drug treatment, as ERK phosphorylation requires LC3-II [67]; we hypothesize that BDMC/Exem treatment decouples LC3-II from p-ERK levels, leading to the independent regulation of both mechanisms.

3.6.2. *St-PGA-$BDMC_1$/$Exem_3$ reduces the levels of paracrine and autocrine signaling molecules*

Cancer cells also secrete autocrine and paracrine factors that promote proliferation, metastasis, and endocrine resistance, such as inflammatory cytokines and exosomes [6,68]. Curcuminoids, including BDMC, have important anti-inflammatory roles and have been widely applied in inflammation-related diseases [12,42]. Exem modulates pro-inflammatory NF-κB signaling, which regulates the levels of multiple cytokines [69]; therefore, Exem and BDMC treatment could also function synergistically through this axis. Additionally, exosomes secreted by cancer cells transport various factors to neighboring and distant cells, which is fundamental to cancer progression and metastasis [70]. We next characterized the levels of the pro-inflammatory cytokines (TNF-α, IL-6, and IL-8) and exosomes secreted into the supernatant of spheroids treated with St-PGA-$BDMC_1$/$Exem_3$ and single-drug conjugates/free drugs (individual/combined) (compared to untreated and DMSO-treated controls).

We failed to observe modulation of TNF-α and IL-6 upon any of the evaluated treatments (Fig. S12A and B). The significant DMSO-induced modulation of IL-8/exosome levels hindered any comparison of BDMC and Exem treatments (individual/combined) with St-PGA-$BDMC_1$/$Exem_3$ (Fig. S12C and 13 - IL-8 and exosome levels after treatment); thus, we focused on IL-8 and exosome release following St-PGA-based treatments.

While St-PGA-$Exem_3$ maintained similar IL-8 levels to untreated controls, St-PGA-$BDMC_1$, a physical mixture of St-PGA-$BDMC_1$ and St-PGA-$Exem_3$, and St-PGA-$BDMC_1$/$Exem_3$ reduced IL-8 levels (Fig. 5I). These results suggest that BDMC drives the reduction of IL-8 levels by the combination conjugate treatment; however, St-PGA-$BDMC_1$/$Exem_3$ significantly reduced IL-8 levels compared to other treatments (Fig. 5I) suggesting the importance of synergistic activity. St-PGA-$Exem_3$ maintained similar exosome levels to controls, while St-PGA-$BDMC_1$, a physical mixture of St-PGA-$BDMC_1$ and St-PGA-$Exem_3$, and St-PGA-$BDMC_1$/$Exem_3$ significantly reduced exosome levels (Fig. 5J). St-PGA-$BDMC_1$/$Exem_3$ exhibited a more significant reduction of exosome levels than individual treatments with St-PGA-$Exem_3$ and St-PGA-$BDMC_1$ (comparable to a physical mixture of St-PGA-$Exem_3$ and St-PGA-$BDMC_1$) suggesting synergistic activity induced by both combination approaches (Fig. 5J). In breast cancer, IL-8 induces remodeling and the epithelial-to-mesenchymal transition, resulting in tumor progression [71,72]; moreover, exosome secretion represents a pivotal means of establishing distant metastases [70]. Thus, decreased IL-8 and exosome levels upon combination conjugate treatment suggest a reduction in tumor progression-related signaling.

Our results suggest that St-PGA-$BDMC_1$/$Exem_3$ simultaneously inhibits Ras/MEK/ERK and PI3K/Akt/mTOR signaling, which may increase therapeutic efficacy/avoid therapeutic resistance via ER-independent pathway activation. We found evidence of synergistic modulation of autophagy as a potential cell death mechanism and synergistic reduction of IL-8/exosome levels, which could inhibit breast cancer progression.

Our characterization of the mechanisms of action of St-PGA-$BDMC_1$/$Exem_3$ and single-drug conjugates/free drugs (individually or combined) supports the benefit of conjugating both drugs to the same polymeric carrier. We hypothesize that the primary mechanism driving the advantages of combination conjugates over physical combinations of single-drug conjugates or free drugs lies in the delivery of drugs to cells at an optimized drug ratio. Thanks to conjugation to the same nanocarrier, drugs will become released within the cell at a rationally selected synergistic ratio, maximizing drug synergism. In contrast, cells will internalize single-drug conjugates or free drugs at independent rates, which can result in a suboptimal drug ratio. The benefits of co-delivering a synergistic combination of drugs, compared to physical mixtures of single-drug conjugates or free drugs, have been previously highlighted [16,17]. The advantage of nanomedicine-based codelivery of synergistic drugs is well-established with the clinical success of Vyxeos®, a liposomal co-encapsulation of synergistic chemotherapeutic agents for acute myeloid leukemia treatment [73]. In agreement with our data, preclinical studies by our laboratory [30,36,74] and others [53,75,76] have highlighted the benefits of conjugating drug combinations to the same polymeric nanocarrier over treatment with physical mixtures of single-drug conjugates/free drugs.

3.7. *Validation of the benefits of St-PGA-based combination conjugates in patient-derived 3D breast cancer organoids*

Patient-derived breast cancer organoids are established from primary tumors and undergo long-term culture [37] while maintaining cell heterogeneity; therefore, they display improved tumor-like characteristics compared to cultures of commercially available cell lines [77,78]. While few studies have applied breast cancer organoids to evaluate nanomedicines despite their growing relevance [34], they represent promising in vitro models that bridge the gap between simplistic cell line-derived models and in vivo evaluations.

We evaluated St-PGA-$BDMC_1$/$Exem_3$ in a hormone-responsive organoid ERC012 (ER+, PR+, HER2-; Fig. S14A and B) established from an untreated tumor (Fig. S14C). We treated ERC012 with St-PGA-$BDMC_1$/$Exem_3$, corresponding single-drug conjugates/free drugs (individually or combined) at the corresponding ratio, imaged organoids at the highest concentrations (98 μM BDMC and 240 μM Exem equivalent; where we expected to find the highest differences between treatments) (Fig. 6A), and reconstructed dose-response curves (Fig. 6B; Fig. S15 - cytotoxicity expressed in Exem equivalent concentration). Table 3 reports IC50 values for each treatment.

Untreated ERC012 organoids presented a round, compact shape with well-defined limits (Fig. 6A; green arrow). ERC012 organoids treated with BDMC and Exem as single agents presented a mix of intact organoids (Fig. 6A; green arrow) and organoids with a partially disaggregated outer layer (Fig. 6A; yellow arrow). As cell death results in a loss of cell-cell interactions, these results suggested cytotoxicity affecting the outer cell layer of the organoid in close contact with the drug-containing media. A physical mixture of St-PGA-$BDMC_1$ and St-PGA-$Exem_3$ or BDMC and Exem provided a comparable result, with a

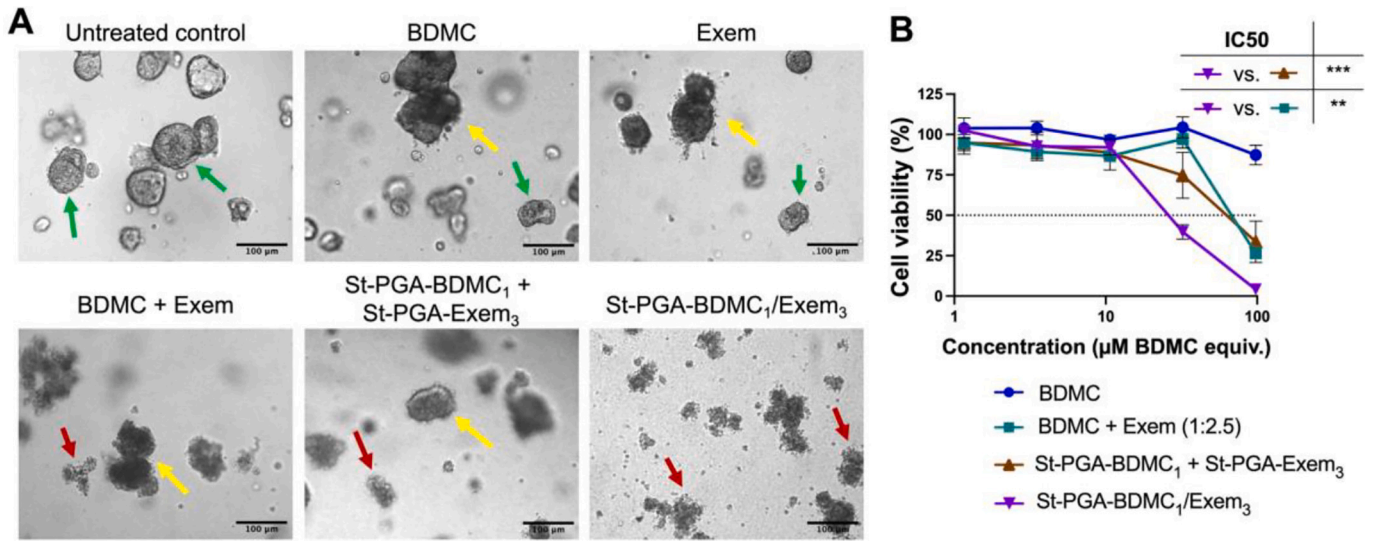

Fig. 6. Cytotoxicity and synergism of St-PGA-BDMC$_1$/Exem$_3$ compared to single-drug conjugates/free drugs in patient-derived hormone-responsive breast cancer organoids. A) Representative images of ERC012 organoids after treatment at 98 µM BDMC and 245 µM equivalent concentrations of PGA-BDMC/Exem used for cytotoxicity assays. Arrows indicate intact organoids (green), apoptotic organoids maintaining integrity (yellow), and apoptotic disaggregated organoids (red). Scale bars = 100 µm. B) Dose-response curves of organoids incubated for 72 h with St-PGA-BDMC$_1$/Exem$_3$, BDMC and Exem at a 1:2.5 ratio, St-PGA-BDMC$_1$ and St-PGA-Exem$_3$ combined at said drug ratio, and free BDMC. Concentrations represented in BDMC-equivalents according to drug loading (Exem-equivalents presented in Fig. S15). Data represented as mean ± SEM of three independent biological replicates ($n = 3$). Statistical analysis performed using an extra sum-of-squared F test fit comparison for IC50 values. Statistical significance for each concentration represented as p-value <0.01 (**) and p-value <0.001 (***). (For interpretation of the references to colour in this figure legend, the reader is referred to the web version of this article.)

Table 3
IC50 values of St-PGA-based conjugates and free drugs in patient-derived organoids.

Compound name	IC50 (µM BDMC Eq.)	IC50 (µM Exem Eq.)	Molar ratio (BDMC:Exem)
BDMC	n/d	n/a	n/a
Exem	n/a	n/d	n/a
BDMC + Exem (1:2.5)	81 ± 1.6	202 ± 1.2	1:2.5
St-PGA-BDMC$_1$/Exem$_3$	27 ± 1.4	68 ± 1.5	1:2.5
St-PGA-BDMC$_1$ + St-PGA-Exem$_3$	67 ± 1.5	167 ± 1.3	1:2.5

BDMC = Bisdemethoxycurcumin; Exem = Exemestane; n/a = not applicable; n/d = not detected.

mix of organoids with a disaggregated outer layer and completely disrupted organoids, suggesting an impact on a more significant number of organoid cell layers (Fig. 6A; red arrow). Only St-PGA-BDMC$_1$/Exem$_3$ treatment prompted complete organoid disruption, suggesting higher cytotoxicity (Fig. 6A). These results suggest that combination-based treatments provided higher cytotoxicity than free drugs and that St-PGA-BDMC$_1$/Exem$_3$ induced more significant cytotoxicity than other combination-based treatments.

To confirm these results, we analyzed dose-response curves at different concentrations (Fig. 6B; Fig. S15). The low cytotoxicity of BDMC and Exem as single drugs impeded statistical analyses and CI curve calculation (Fig. 6B; Fig. S15); nevertheless, combination-based strategies resulted in more significant cytotoxicity than free drugs as individual treatments, suggesting synergism in patient-derived breast cancer organoids (Fig. 6B; Fig. S15). St-PGA-BDMC$_1$/Exem$_3$ induced higher cytotoxicity than a physical mixture of St-PGA-BDMC$_1$ and St-PGA-Exem$_3$ or BDMC and Exem (Fig. 6B; Fig. S15). Thus, St-PGA-BDMC$_1$/Exem$_3$ induced significantly higher cytotoxicity than alternative combination strategies, highlighting the benefit of conjugating both drugs to the same St-PGA carrier in a patient-derived model and validating preliminary results obtained in cell monolayers and spheroids (Fig. 1B). The combination conjugate St-PGA-BDMC$_1$/Exem$_3$ outperformed all treatments in patient-derived organoids, displaying better cytotoxicity results than in cell spheroids (Fig. 5C). Thus, patient-derived organoids recapitulated further advantages of combination conjugates than cell line-derived spheroids. These results revealed that more complex models supported the benefit of combination conjugates over physical mixtures of single-drug conjugates/free drugs.

Overall, the present work highlights the importance of rational selection of candidates supported in advanced in vitro models. The routinary implementation of advanced in vitro models, such as patient-derived breast cancer organoids, can reduce animal model use, which aligns with the European Commission's 3R goals [79]. To the best of our knowledge, only one report previously applied patient-derived breast cancer organoids to the development of a novel nanomedicine-based therapeutic [80]. Our results further underscore the potential of advanced preclinical models in validating novel, promising breast cancer therapeutics.

Multiple preclinical studies already supported the potential of PGA-based conjugates [30,53,75,81,82]. Additionally, the clinical evaluation of Opaxio®, PGA-conjugated paclitaxel, demonstrated safety advantages and supported the further clinical exploration of PGA-based conjugates despite not reaching regulatory approval for various solid tumors [83–85]. St-PGA-based conjugates possess several advantages compared to their linear counterparts, such as improved biodistribution, pharmacokinetics, and cell trafficking [26]. In agreement with our previous St-PGA-based conjugates for single-drug [23] and combination therapy [74], the results for St-PGA-BDMC$_1$/Exem$_3$ underscore the potential of St-PGA-based conjugates for breast cancer combination treatment.

4. Conclusions

Herein, we report a rationally designed St-PGA-based combination conjugate carrying BDMC and Exem as a potentially effective advanced hormone-responsive breast cancer treatment. We explored a variety of drug loadings and combination ratios, utilizing pH-responsive ester and hydrazone linkers for BDMC and Exem conjugation, respectively. Our characterization highlighted the impact of drug loading and composition on the size distribution and solution conformation of the resulting

conjugates, significantly influencing the kinetics of drug(s) release profiles under acidic environments. Drug synergism was determined in cell models of increasing complexity with the validation of the best rational design in patient-derived 3D organoids, demonstrating that combination conjugates displayed significant benefits compared to the single mixture counterparts. Notably, a combination conjugate (at the lowest drug loading) outperformed the remaining conjugates in terms of cytotoxicity/synergism. The selected candidate (St-PGA-$BDMC_1$/$Exem_3$) synergistically inhibited proliferation pathways and inflammatory chemokine/exosome release but increased autophagy. St-PGA-$BDMC_1$/$Exem_3$ also outperformed a physical mixture of single-drug conjugates/free drugs in patient-derived organoids. Overall, we successfully applied rational design and selection using in vitro models of increasing complexity to obtain a promising St-PGA-based combination conjugate for hormone-responsive breast cancer treatment that we aim to evaluate in vivo in the future.

CRediT authorship contribution statement

Paz Boix-Montesinos: Writing – original draft, Methodology, Investigation, Formal analysis, Data curation. **María Medel:** Writing – review & editing, Methodology, Investigation, Data curation. **Alessio Malfanti:** Writing – review & editing, Methodology, Investigation, Data curation. **Snežana Đorđević:** Writing – review & editing, Methodology, Investigation, Data curation. **Esther Masiá:** Writing – review & editing, Methodology, Investigation, Data curation. **David Charbonnier:** Investigation, Methodology. **Paula Carrascosa-Marco:** Methodology, Investigation. **Ana Armiñán:** Writing – review & editing, Validation, Supervision, Formal analysis, Conceptualization. **María J. Vicent:** Writing – review & editing, Validation, Supervision, Resources, Project administration, Funding acquisition, Conceptualization.

Data availability

Data will be made available on request.

Acknowledgments

The authors thank Dr. Stuart P. Atkinson for English revision, critical feedback, and his aid in manuscript development. This work was supported by the European Research Council (grant ERC-CoG-2014-648831 "MyNano" to M.J.V.); the Spanish Ministry of Science, Innovation, and Universities (PID2019-108806RB-I00, P.B-M. FPU grant FPU18/00386) and CIBERONC (project n. CB22/12/00048). Part of the equipment employed in this work has been funded by Generalitat Valenciana and co-financed with FEDER funds (PO FEDER of Comunitat Valenciana 2014–2020). The authors acknowledge Dr. Jose Antonio López-Guerrero and Dr. Ana Calatrava-Fons (FIVO, Valencia, Spain) for breast tumor tissue donation. The authors acknowledge the use of Biorender.com in the graphical abstract.

Appendix A. Supplementary data

Supplementary data to this article can be found online at https://doi.org/10.1016/j.jconrel.2024.09.002.

References

[1] A. Burguin, C. Diorio, F. Durocher, Breast cancer treatments: updates and new challenges, J. Pers. Med. 11 (2021), https://doi.org/10.3390/jpm11080808.
[2] A.G. Waks, E.P. Winer, Breast Cancer treatment: a review, JAMA 321 (2019) 288–300, https://doi.org/10.1001/jama.2018.19323.
[3] E. Nolan, G.J. Lindeman, J.E. Visvader, Deciphering breast cancer: from biology to the clinic, Cell (2023), https://doi.org/10.1016/j.cell.2023.01.040.
[4] L. Clusan, F. Ferrière, G. Flouriot, F. Pakdel, A basic review on estrogen receptor signaling pathways in breast Cancer, Int. J. Mol. Sci. 24 (2023), https://doi.org/10.3390/ijms24076834.
[5] N. Bahrami, G. Chang, N. Kanaya, T. Sauer, D. Park, M. Loeng, B. Gravdehaug, S. Chen, J. Geisler, Changes in serum estrogenic activity during neoadjuvant therapy with letrozole and exemestane, J. Steroid Biochem. Mol. Biol. 200 (2020) 105641, https://doi.org/10.1016/J.JSBMB.2020.105641.
[6] A.B. Hanker, D.R. Sudhan, C.L. Arteaga, Overcoming endocrine resistance in breast Cancer, Cancer Cell 37 (2020) 496–513, https://doi.org/10.1016/J.CCELL.2020.03.009.
[7] T.V. Augusto, C. Amaral, C.F. Almeida, N. Teixeira, G. Correia-da-Silva, Differential biological effects of aromatase inhibitors: apoptosis, autophagy, senescence and modulation of the hormonal status in breast cancer cells, Mol. Cell. Endocrinol. 537 (2021), https://doi.org/10.1016/j.mce.2021.111426.
[8] C. Amaral, M. Borges, S. Melo, E.T. da Silva, G. Correia-da-Silva, N. Teixeira, Apoptosis and autophagy in breast cancer cells following exemestane treatment, PLoS One 7 (2012), https://doi.org/10.1371/journal.pone.0042398.
[9] C. Amaral, T.V. Augusto, M. Almada, S.C. Cunha, G. Correia-da-Silva, N. Teixeira, The potential clinical benefit of targeting androgen receptor (AR) in estrogen-receptor positive breast cancer cells treated with Exemestane, Biochim. Biophys. Acta Mol. basis Dis. 1866 (2020), https://doi.org/10.1016/j.bbadis.2019.165661.
[10] C. Amaral, T.V. Augusto, E. Tavares-da-Silva, F.M.F. Roleira, G. Correia-da-Silva, N. Teixeira, Hormone-dependent breast cancer: targeting autophagy and PI3K overcomes Exemestane-acquired resistance, J. Steroid Biochem. Mol. Biol. 183 (2018), https://doi.org/10.1016/j.jsbmb.2018.05.006.
[11] H. Wang, Y. Huang, Combination therapy based on nano codelivery for overcoming cancer drug resistance, Med. Drug Discov. 6 (2020), https://doi.org/10.1016/j.medidd.2020.100024.
[12] P. Joshi, S. Joshi, D. Semwal, A. Bisht, S. Paliwal, J. Dwivedi, S. Sharma, Curcumin: an insight into molecular pathways involved in anticancer activity, Mini-reviews Med. Chem. 21 (2021) 2420–2457, https://doi.org/10.2174/1389557521666210122153823.
[13] S. Wünsche, L. Yuan, A. Seidel-Morgenstern, H. Lorenz, A contribution to the solid state forms of bis(Demethoxy)curcumin: co-crystal screening and characterization, Molecules 26 (2021), https://doi.org/10.3390/molecules26030720.
[14] S. Rampogu, S.M. Kim, M. Son, A. Baek, C. Park, G. Lee, Y. Kim, G.S. Kim, J.H. Kim, K.W. Lee, A computational approach with biological evaluation: combinatorial treatment of curcumin and exemestane synergistically regulates ddx3 expression in cancer cell lines, Biomolecules 10 (2020), https://doi.org/10.3390/biom10060857.
[15] S. Chaturvedi, A. Garg, A comprehensive review on novel delivery approaches for exemestane, J. Drug Deliv. Sci. Technol. 75 (2022) 103655, https://doi.org/10.1016/J.JDDST.2022.103655.
[16] D.R. Vogus, V. Krishnan, S. Mitragotri, A review on engineering polymer drug conjugates to improve combination chemotherapy, Curr. Opin. Colloid Interface Sci. 31 (2017) 75–85, https://doi.org/10.1016/J.COCIS.2017.08.002.
[17] F. Greco, M.J. Vicent, Combination therapy: opportunities and challenges for polymer-drug conjugates as anticancer nanomedicines, Adv. Drug Deliv. Rev. 61 (2009) 1203–1213, https://doi.org/10.1016/j.addr.2009.05.006.
[18] A.S. Ombredane, V.R.P. Silva, L.R. Andrade, W.O. Pinheiro, M. Simonelly, J. V. Oliveira, A.C. Pinheiro, G.F. Gonçalves, G.J. Felice, M.P. Garcia, P.M. Campos, G.V.S. Luz, G.A. Joanitti, In vivo efficacy and toxicity of curcumin nanoparticles in breast Cancer treatment: a systematic review, Front. Oncol. 11 (2021), https://doi.org/10.3389/fonc.2021.612903.
[19] S. Patel, J. Kim, M. Herrera, A. Mukherjee, A.V. Kabanov, G. Sahay, Brief update on endocytosis of nanomedicines, Adv. Drug Deliv. Rev. 144 (2019), https://doi.org/10.1016/j.addr.2019.08.004.
[20] O. Zagorodko, J.J. Arroyo-Crespo, V.J. Nebot, M.J. Vicent, Polypeptide-based conjugates as therapeutics: opportunities and challenges, Macromol. Biosci. 17 (2017), https://doi.org/10.1002/mabi.201600316.
[21] T. Melnyk, S. Đorđević, I. Conejos-Sánchez, M.J. Vicent, Therapeutic potential of polypeptide-based conjugates: rational design and analytical tools that can boost clinical translation, Adv. Drug Deliv. Rev. 160 (2020), https://doi.org/10.1016/j.addr.2020.10.007.
[22] A. Duro-Castano, I. Conejos-Sánchez, M.J. Vicent, Peptide-based polymer therapeutics, Polymers (Basel) 6 (2014) 515–551, https://doi.org/10.3390/polym6020515.
[23] T. Melnyk, E. Masiá, O. Zagorodko, I. Conejos-Sánchez, M.J. Vicent, Rational design of poly-L-glutamic acid-palbociclib conjugates for pediatric glioma treatment, J. Control. Release 355 (2023), https://doi.org/10.1016/j.jconrel.2023.01.079.
[24] J. Yang, J. Kopeček, The light at the end of the tunnel—second generation HPMA conjugates for cancer treatment, Curr. Opin. Colloid Interface Sci. 31 (2017), https://doi.org/10.1016/j.cocis.2017.07.003.
[25] I. Ekladious, Y.L. Colson, M.W. Grinstaff, Polymer–drug conjugate therapeutics: advances, insights and prospects, Nat. Rev. Drug Discov. 18 (2019), https://doi.org/10.1038/s41573-018-0005-0.
[26] L.I.F. Moura, A. Malfanti, C. Peres, A.I. Matos, E. Guegain, V. Sainz, M. Zloh, M. J. Vicent, H.F. Florindo, Functionalized branched polymers: promising immunomodulatory tools for the treatment of cancer and immune disorders, Mater. Horiz. 6 (2019), https://doi.org/10.1039/c9mh00628a.
[27] A. Aurelia Chis, C. Dobrea, C. Morgovan, A.M. Arseniu, L.L. Rus, A. Butuca, A. M. Juncan, M. Totan, A.L. Vonica-Tincu, G. Cormos, A.C. Muntean, M.L. Muresan, F.G. Gligor, A. Frum, Applications and limitations of dendrimers in biomedicine, Molecules 25 (2020), https://doi.org/10.3390/molecules25173982.
[28] A. Duro-Castano, V.J. Nebot, A. Niño-Pariente, A. Armiñán, J.J. Arroyo-Crespo, A. Paul, N. Feiner-Gracia, L. Albertazzi, M.J. Vicent, Capturing "extraordinary" soft-assembled charge-like polypeptides as a strategy for Nanocarrier design, Adv. Mater. 29 (2017), https://doi.org/10.1002/adma.201702888.

[29] A. Duro-Castano, R.M. England, D. Razola, E. Romero, M. Oteo-Vives, M. A. Morcillo, M.J. Vicent, Well-defined star-shaped polyglutamates with improved pharmacokinetic profiles as excellent candidates for biomedical applications, Mol. Pharm. 12 (2015), https://doi.org/10.1021/acs.molpharmaceut.5b00358.

[30] J.J. Arroyo-Crespo, A. Armiñán, D. Charbonnier, L. Balzano-Nogueira, F. Huertas-López, C. Martí, S. Tarazona, J. Forteza, A. Conesa, M.J. Vicent, Tumor microenvironment-targeted poly-L-glutamic acid-based combination conjugate for enhanced triple negative breast cancer treatment, Biomaterials 186 (2018) 8–21, https://doi.org/10.1016/J.BIOMATERIALS.2018.09.023.

[31] M.J. Vicent, F. Greco, R.I. Nicholson, A. Paul, P.C. Griffiths, R. Duncan, Polymer therapeutics designed for a combination therapy of hormone-dependent cancer, Angew. Chem. Int. Ed. 44 (2005), https://doi.org/10.1002/anie.200462960.

[32] J.M. Metselaar, T. Lammers, Challenges in nanomedicine clinical translation, Drug Deliv. Transl. Res. 10 (2020), https://doi.org/10.1007/s13346-020-00740-5.

[33] M.A. Younis, H.M. Tawfeek, A.A.H. Abdellatif, J.A. Abdel-Aleem, H. Harashima, Clinical translation of nanomedicines: challenges, opportunities, and keys, Adv. Drug Deliv. Rev. 181 (2022) 114083, https://doi.org/10.1016/J.ADDR.2021.114083.

[34] D.K. Zhao, J. Liang, X.Y. Huang, S. Shen, J. Wang, Organoids technology for advancing the clinical translation of cancer nanomedicine, Wiley Interdiscip. Rev. Nanomed. Nanobiotechnol. 15 (2023), https://doi.org/10.1002/wnan.1892.

[35] S. Pozzi, A. Scomparin, S. Israeli Dangoor, D. Rodriguez Ajamil, P. Ofek, L. Neufeld, A. Krivitsky, D. Vaskovich-Koubi, R. Kleiner, P. Dey, S. Koshrovski-Michael, N. Reisman, R. Satchi-Fainaro, Meet me halfway: are in vitro 3D cancer models on the way to replace in vivo models for nanomedicine development? Adv. Drug Deliv. Rev. 175 (2021) https://doi.org/10.1016/j.addr.2021.04.001.

[36] G. Córdoba-David, A. Duro-Castano, R.C. Castelo-Branco, C. González-Guerrero, P. Cannata, A.B. Sanz, M.J. Vicent, A. Ortiz, A.M. Ramos, Effective Nephroprotection against acute kidney injury with a star-shaped Polyglutamate-Curcuminoid conjugate, Sci. Rep. 10 (2020), https://doi.org/10.1038/s41598-020-58974-9.

[37] N. Sachs, J. de Ligt, O. Kopper, E. Gogola, G. Bounova, F. Weeber, A.V. Balgobind, K. Wind, A. Gracanin, H. Begthel, J. Korving, R. van Boxtel, A.A. Duarte, D. Lelieveld, A. van Hoeck, R.F. Ernst, F. Blokzijl, I.J. Nijman, M. Hoogstraat, M. van de Ven, D.A. Egan, V. Zinzalla, J. Moll, S.F. Boj, E.E. Voest, L. Wessels, P. J. van Diest, S. Rottenberg, R.G.J. Vries, E. Cuppen, H. Clevers, A living biobank of breast Cancer organoids captures disease heterogeneity, Cell (2018), https://doi.org/10.1016/j.cell.2017.11.010.

[38] S. Zheng, W. Wang, J. Aldahdooh, A. Malyutina, T. Shadbahr, Z. Tanoli, A. Pessia, J. Tang, SynergyFinder plus: toward better interpretation and annotation of drug combination screening datasets, Genom. Proteom. Bioinformat. 20 (2022), https://doi.org/10.1016/j.gpb.2022.01.004.

[39] T. Sun, C. Jiang, Stimuli-responsive drug delivery systems triggered by intracellular or subcellular microenvironments, Adv. Drug Deliv. Rev. 196 (2023) 114773, https://doi.org/10.1016/J.ADDR.2023.114773.

[40] J. Shinn, N. Kwon, S.A. Lee, Y. Lee, Smart pH-responsive nanomedicines for disease therapy, J. Pharm. Investig. 52 (2022), https://doi.org/10.1007/s40005-022-00573-z.

[41] T.N. Le, V.R. Neralla, Evaluation of the best pH-sensitive linker using norbornene-derived polymers, journal of macromolecular science, Part A: Pure Appl. Chem. 58 (2021), https://doi.org/10.1080/10601325.2020.1858717.

[42] C.M. Cuesta, F. Ibañez, R. Lopez-Hidalgo, J. Ureña, A. Duro-Castano, A. Armiñán, M.J. Vicent, M. Pascual, C. Guerri, A targeted polypeptide-based nanoconjugate as a nanotherapeutic for alcohol-induced neuroinflammation, Nanomedicine 34 (2021), https://doi.org/10.1016/j.nano.2021.102376.

[43] A. Duro-Castano, C. Borrás, V. Herranz-Pérez, M.C. Blanco-Gandía, I. Conejos-Sánchez, A. Armiñán, C. Mas-Bargues, M. Inglés, J. Miñarro, M. Rodríguez-Arias, J. M. García-Verdugo, J. Viña, M.J. Vicent, Targeting Alzheimer's disease with multimodal polypeptide-based nanoconjugates, Sci. Adv. 7 (2021), https://doi.org/10.1126/sciadv.abf9180.

[44] S.J. Sonawane, R.S. Kalhapure, T. Govender, Hydrazone linkages in pH responsive drug delivery systems, Eur. J. Pharm. Sci. 99 (2017), https://doi.org/10.1016/j.ejps.2016.12.011.

[45] F.M. Veronese, O. Schiavon, G. Pasut, R. Mendichi, L. Andersson, A. Tsirk, J. Ford, G. Wu, S. Kneller, J. Davies, R. Duncan, PEG-doxorubicin conjugates: influence of polymer structure on drug release, in vitro cytotoxicity, biodistribution, and antitumor activity, Bioconjug. Chem. 16 (2005), https://doi.org/10.1021/bc040241m.

[46] J. Caciolla, A. Spinello, S. Martini, A. Bisi, N. Zaffaroni, S. Gobbi, A. Magistrato, Targeting Orthosteric and allosteric pockets of aromatase via dual-mode novel azole inhibitors, ACS Med. Chem. Lett. 11 (2020), https://doi.org/10.1021/acsmedchemlett.9b00591.

[47] J.S. Wright, Predicting the antioxidant activity of curcumin and curcuminoids, J. Mol. Struct. (THEOCHEM) 591 (2002), https://doi.org/10.1016/S0166-1280(02)00242-7.

[48] K.I. Priyadarsini, The chemistry of curcumin: from extraction to therapeutic agent, Molecules 19 (2014), https://doi.org/10.3390/molecules191220091.

[49] W.R. Zhuang, Y. Wang, P.F. Cui, L. Xing, J. Lee, D. Kim, H.L. Jiang, Y.K. Oh, Applications of π-π stacking interactions in the design of drug-delivery systems, J. Control. Release 294 (2019), https://doi.org/10.1016/j.jconrel.2018.12.014.

[50] T. Etrych, V. Šubr, R. Laga, B. Říhová, K. Ulbrich, Polymer conjugates of doxorubicin bound through an amide and hydrazone bond: impact of the carrier structure onto synergistic action in the treatment of solid tumours, Eur. J. Pharm. Sci. 58 (2014) 1–12, https://doi.org/10.1016/J.EJPS.2014.02.016.

[51] J. Halder, D. Pradhan, B. Kar, G. Ghosh, G. Rath, Nanotherapeutics approaches to overcome P-glycoprotein-mediated multi-drug resistance in cancer, Nanomedicine 40 (2022), https://doi.org/10.1016/j.nano.2021.102494.

[52] V.B. Junyaprasert, P. Thummarati, Innovative design of targeted nanoparticles: polymer–drug conjugates for enhanced cancer therapy, Pharmaceutics 15 (2023), https://doi.org/10.3390/pharmaceutics15092216.

[53] E. Markovsky, H. Baabur-Cohen, R. Satchi-Fainaro, Anticancer polymeric nanomedicine bearing synergistic drug combination is superior to a mixture of individually-conjugated drugs, J. Control. Release 187 (2014), https://doi.org/10.1016/j.jconrel.2014.05.025.

[54] M. Moniruzzaman, A. Karthikeyan, J. Yakubu, A.V. Pandey, Innovative Delivery Systems for Curcumin: Exploring Nanosized and Conventional Formulations, 2024, https://doi.org/10.3390/pharmaceutics.

[55] G. Bahcecioglu, G. Basara, B.W. Ellis, X. Ren, P. Zorlutuna, Breast cancer models: engineering the tumor microenvironment, Acta Biomater. 106 (2020) 1–21, https://doi.org/10.1016/j.actbio.2020.02.006.

[56] G. Lazzari, P. Couvreur, S. Mura, Multicellular tumor spheroids: a relevant 3D model for the: in vitro preclinical investigation of polymer nanomedicines, Polym. Chem. 8 (2017), https://doi.org/10.1039/c7py00559h.

[57] X. He, Y. Yang, Y. Han, C. Cao, Z. Zhang, L. Li, C. Xiao, H. Guo, L. Wang, L. Han, Z. Qu, N. Liu, S. Han, F. Xu, Extracellular matrix physical properties govern the diffusion of nanoparticles in tumor microenvironment, Proc. Natl. Acad. Sci. USA 120 (2023), https://doi.org/10.1073/pnas.2209260120.

[58] M.U. Munir, Nanomedicine penetration to tumor: challenges, and advanced strategies to tackle this issue, Cancers (Basel) 14 (2022), https://doi.org/10.3390/cancers14122904.

[59] A. Shakeri, A.F.G. Cicero, Y. Panahi, M. Mohajeri, A. Sahebkar, Curcumin: a naturally occurring autophagy modulator, J. Cell. Physiol. 234 (2019), https://doi.org/10.1002/jcp.27404.

[60] H.Y. Lin, J.N. Lin, J.W. Ma, N.S. Yang, C.T. Ho, S.C. Kuo, T. Der Way, Demethoxycurcumin induces autophagic and apoptotic responses on breast cancer cells in photodynamic therapy, J. Funct. Foods 12 (2015) 439–449, https://doi.org/10.1016/J.JFF.2014.12.014.

[61] Y.K. Lee, J.A. Lee, Role of the mammalian ATG8/LC3 family in autophagy: differential and compensatory roles in the spatiotemporal regulation of autophagy, BMB Rep. 49 (2016), https://doi.org/10.5483/BMBRep.2016.49.8.081.

[62] A. Rocca, L. Braga, M.C. Volpe, S. Maiocchi, D. Generali, The predictive and prognostic role of RAS–RAF–MEK–ERK pathway alterations in breast Cancer: revision of the literature and comparison with the analysis of Cancer genomic datasets, Cancers (Basel) 14 (2022), https://doi.org/10.3390/cancers14215306.

[63] N. Mizushima, T. Yoshimori, How to interpret LC3 immunoblotting, Autophagy 3 (2007), https://doi.org/10.4161/auto.4600.

[64] B. Nuvoli, E. Camera, A. Mastrofrancesco, S. Briganti, R. Galati, Modulation of reactive oxygen species via ERK and STAT3 dependent signalling are involved in the response of mesothelioma cells to exemestane, Free Radic. Biol. Med. 115 (2018) 266–277, https://doi.org/10.1016/J.FREERADBIOMED.2017.12.008.

[65] Z. Pan, H. Zhang, S. Dokudovskaya, The role of mTORC1 pathway and autophagy in resistance to platinum-based chemotherapeutics, Int. J. Mol. Sci. 24 (2023), https://doi.org/10.3390/ijms241310651.

[66] S.H. Hare, A.J. Harvey, mTOR function and therapeutic targeting in breast cancer, Am. J. Cancer Res. 7 (2017).

[67] N. Martinez-Lopez, D. Athonvarangkul, P. Mishall, S. Sahu, R. Singh, Autophagy proteins regulate ERK phosphorylation, Nat. Commun. 4 (2013), https://doi.org/10.1038/ncomms3799.

[68] T.B. Steinbichler, J. Dudás, H. Riechelmann, I.I. Skvortsova, The role of exosomes in cancer metastasis, Semin. Cancer Biol. 44 (2017) 170–181, https://doi.org/10.1016/j.semcancer.2017.02.006.

[69] T. Liu, L. Zhang, D. Joo, S.C. Sun, NF-κB signaling in inflammation, Signal Transduct. Target. Ther. 2 (2017), https://doi.org/10.1038/sigtrans.2017.23.

[70] C. Giordano, G. La Camera, L. Gelsomino, I. Barone, D. Bonofiglio, S. Andò, S. Catalano, The biology of exosomes in breast cancer progression: dissemination, immune evasion and metastatic colonization, Cancers (Basel) 12 (2020), https://doi.org/10.3390/cancers12082179.

[71] K. Fousek, L.A. Horn, C. Palena, Interleukin-8: a chemokine at the intersection of cancer plasticity, angiogenesis, and immune suppression, Pharmacol. Ther. 219 (2021), https://doi.org/10.1016/j.pharmthera.2020.107692.

[72] N. Todorović-Raković, J. Milovanović, Interleukin-8 in breast cancer progression, J. Interf. Cytokine Res. 33 (2013), https://doi.org/10.1089/jir.2013.0023.

[73] A.W. Tolcher, L.D. Mayer, Improving combination cancer therapy: the CombiPlex® development platform, Future Oncol. 14 (2018), https://doi.org/10.2217/fon-2017-0607.

[74] A. Lepland, A. Malfanti, U. Haljasorg, E.K. Asciutto, M. Pickholz, M. Bringas, S. Đorđević, L. Salumäe, P. Peterson, T. Teesalu, M.J. Vicent, P. Scodeller, Depletion of mannose receptor–positive tumor-associated macrophages via a peptide-targeted star-shaped polyglutamate inhibits breast cancer progression in mice, Cancer Res. Commun. 2 (2022), https://doi.org/10.1158/2767-9764.crc-22-0043.

[75] H. Baabur-Cohen, L.I. Vossen, H.R. Krüger, A. Eldar-boock, E. Yeini, N. Landa-Rouben, G. Tiram, S. Wedepohl, E. Markovsky, J. Leor, M. Calderón, R. Satchi-Fainaro, In vivo comparative study of distinct polymeric architectures bearing a combination of paclitaxel and doxorubicin at a synergistic ratio, J. Control. Release 257 (2017) 118–131, https://doi.org/10.1016/J.JCONREL.2016.06.037.

[76] D.R. Vogus, M.A. Evans, A. Pusuluri, A. Barajas, M. Zhang, V. Krishnan, M. Nowak, S. Menegatti, M.E. Helgeson, T.M. Squires, S. Mitragotri, A hyaluronic acid conjugate engineered to synergistically and sequentially deliver gemcitabine and

doxorubicin to treat triple negative breast cancer, J. Control. Release 267 (2017), https://doi.org/10.1016/j.jconrel.2017.08.016.
[77] J. Drost, H. Clevers, Organoids in cancer research, Nat. Rev. Cancer (2018), https://doi.org/10.1038/s41568-018-0007-6.
[78] B.L. LeSavage, R.A. Suhar, N. Broguiere, M.P. Lutolf, S.C. Heilshorn, Next-generation cancer organoids, Nat. Mater. 21 (2022), https://doi.org/10.1038/s41563-021-01057-5.
[79] D.M. Stresser, A.K. Kopec, P. Hewitt, R.N. Hardwick, T.R. Van Vleet, P.K. S. Mahalingaiah, D. O'Connell, G.J. Jenkins, R. David, J. Graham, D. Lee, J. Ekert, A. Fullerton, R. Villenave, P. Bajaj, J.R. Gosset, S.L. Ralston, M. Guha, A. Amador-Arjona, K. Khan, S. Agarwal, C. Hasselgren, X. Wang, K. Adams, G. Kaushik, A. Raczynski, K.A. Homan, Towards in vitro models for reducing or replacing the use of animals in drug testing, Nat. Biomed. Eng. (2023), https://doi.org/10.1038/s41551-023-01154-7.
[80] B. Li, F. Qi, F. Zhu, Z. Lu, M. Wang, T. Chu, S. Wu, J. Wei, Z. Song, S. Sukumar, C. Zhang, J. Xu, S. Li, G. Nie, Nanoparticle-based combination therapy enhances Fulvestrant efficacy and overcomes tumor resistance in ER-positive breast Cancer, Cancer Res. 83 (2023), https://doi.org/10.1158/0008-5472.CAN-22-3559.
[81] E. Pisarevsky, R. Blau, Y. Epshtein, D. Ben-Shushan, A. Eldar-Boock, G. Tiram, S. Koshrovski-Michael, A. Scomparin, S. Pozzi, A. Krivitsky, G. Shenbach-Koltin, E. Yeini, L. Fridrich, R. White, R. Satchi-Fainaro, Rational Design of Polyglutamic Acid Delivering an optimized combination of drugs targeting mutated BRAF and MEK in melanoma, Adv. Ther. (Weinh) 3 (2020), https://doi.org/10.1002/adtp.202000028.
[82] S. Đorđević, M. Medel, J. Hillaert, E. Masiá, I. Conejos-Sánchez, M.J. Vicent, Critical design strategies supporting optimized drug release from polymer–drug conjugates, Small 20 (2024), https://doi.org/10.1002/smll.202303157.
[83] K.S. Albain, C.P. Belani, P. Bonomi, K.J. O'Byrne, J.H. Schiller, M. Socinski, Pioneer: a phase III randomized trial of paclitaxel poliglumex versus paclitaxel in chemotherapy-naive women with advanced-stage non-small-cell lung cancer and performance status of 2, Clin. Lung Cancer 7 (2006), https://doi.org/10.3816/CLC.2006.n.027.
[84] T.M. Beer, C. Ryan, J. Alumkal, C.W. Ryan, J. Sun, K.M. Eilers, A phase II study of paclitaxel poliglumex in combination with transdermal estradiol for the treatment of metastatic castration-resistant prostate cancer after docetaxel chemotherapy, Anti-Cancer Drugs 21 (2010), https://doi.org/10.1097/CAD.0b013e3283355211.
[85] C.J. Langer, K.J. O'Byrne, M.A. Socinski, S.M. Mikhailov, K. Leśniewski-Kmak, M. Smakal, T.E. Ciuleanu, S.V. Orlov, M. Dediu, D. Heigener, A.J. Eisenfeld, L. Sandalic, F.B. Oldham, J.W. Singer, H.J. Ross, Phase III trial comparing paclitaxel Poliglumex (CT-2103, PPX) in combination with carboplatin versus standard paclitaxel and carboplatin in the treatment of PS 2 patients with chemotherapy-Naïve advanced non-small cell lung Cancer, J. Thorac. Oncol. 3 (2008) 623–630, https://doi.org/10.1097/JTO.0B013E3181753B4B.